The impact of geochemical and life-cycle variables on carbon dioxide removal by enhanced rock weathering: Development and application of the Stella ERW model

James Jerden [a,1,*], Meteb Mejbel [a], Antonio Nilson Zamunér Filho [b], Monica Carroll [c], Joanna Campe [a]

[a] *Remineralize the Earth, 152 South Street, Northampton, MA, 01060, USA*
[b] *Faculty of Engineering, Federal University of Catalão, Av. Dr. Lamartine Pinto de Avelar, 1.120, Catalão, 75704-020, GO, Brazil*
[c] *University Library, University of Illinois Urbana-Champaign, 507 East Green Street, Champaign, IL, 61820, USA*

ABSTRACT

The carbon dioxide removal (CDR) potential of enhanced rock weathering (ERW) depends on dynamic interactions between several biogeochemical and life-cycle variables. This paper reports results from a systems model developed to account for key variable interactions and provide a computational tool for optimizing ERW applications. We discuss the model development, comparisons with laboratory and field test data, and results from a series of sensitivity analyses for several hypothetical ERW applications. The simulations were performed using a model developed in Stella Architect, an object-oriented systems dynamics modeling code. The model tracks the amount of carbon dioxide consumed by the weathering of a user-specified mass of rock powder in a soil environment. The primary model variables are: rock powder particle size distribution, soil pH, soil temperature, soil pore water saturation index, and a biological weathering factor. The rock bulk composition is also a key variable as it defines the enhanced weathering potential of the rock powder. Life cycle variables such as carbon emissions from mining, rock crushing, and transport are also quantified. The model predictions are consistent with measured data. It predicts CDR values ranging from 1 to 12 t CO_2 ha^{-1} (depending on conditions) for single applications of 20–40 t of rock ha^{-1} over a 10-year interval. Applying the model to a hypothetical large-scale ERW campaign in which basalt rock powder is applied to 25% and 75% of Brazilian cropland results in CDR values of 0.15 and 0.5 Gt CO_2 over ten years, respectively (for a single application). Model results show that combinations of suboptimal rock type (i.e., low concentrations of divalent cations and slow weathering rates for field conditions) and suboptimal life-cycle variables (i.e., high vehicle emission factors and long rock transport distances) can result in net positive CO_2 emissions for some hypothetical ERW scenarios. It is, therefore, emphasized that the quantitative co-optimization of geochemical, biological, and life-cycle variables is essential in the planning stages of ERW applications.

1. Introduction

To mitigate the ecological damage and human hardship caused by climate change, the United Nations Intergovernmental Panel on Climate Change (IPCC) has established a goal of limiting global warming to less than 1.5°C relative to preindustrial levels (IPCC, 2018). In their 2022 report on mitigating climate change, the IPCC emphasized that achieving net-zero emissions and maintaining global temperatures

below the 1.5°C threshold will require active carbon dioxide removal to counterbalance hard-to-abate residual sources of CO_2 (IPCC 2022; Box TS.10.). One of the most promising large-scale carbon dioxide removal (CDR) methodologies is enhanced rock weathering (ERW), also referred to as enhanced weathering (EW), terrestrial enhanced weathering (TEW) or enhanced mineral weathering (EMW).

The weathering of silicate rock is the dominant natural CO_2 removal process over geologic time scales (Arrhenius and Holden, 1897; Urey,

---

* Corresponding author.
  E-mail address: jerden@wisc.edu (J. Jerden).
[1] Current address: Sustainability Research Hub, Nelson Institute for Environmental Studies and Office of Sustainability, University of Wisconsin-Madison, 21 N Park St Madison, WI 53715, USA.

1952; Walker et al., 1981; Berner et al., 1983; Brantley et al., 2023). Practitioners of ERW accelerate this natural CDR process by applying finely ground (high reactive surface area) rock powder to soils and coastal environments. This paper focuses on the terrestrial application of ERW to agricultural soils. The use of terrestrial ERW for carbon dioxide removal has been discussed and studied for decades (e.g., Seifritz, 1990; Goldberg et al., 2001; Schuiling and Krijgsman, 2006; Köhler et al., 2010; Renforth, 2012; Hartmann et al., 2013a, b; Manning and Renforth, 2013; Moosdorf et al., 2014; Taylor et al., 2016; Edwards et al., 2017; Kantola et al., 2017; Meysman and Montserrat, 2017; Taylor et al., 2017; Strefler et al., 2018; Renforth, 2019; Lefebvre et al., 2019; Lehmann and Possinger, 2020; Beerling et al., 2020; Kelland et al., 2020; Goll et al., 2021; Vakilifard et al., 2021; Lewis et al., 2021; Haque et al., 2021; Rinder and von Hagke, 2021; Kemp et al., 2022; Vicca et al., 2022; Kantzas et al., 2022; Stubbs et al., 2022; Eufrasio et al., 2022; Zhang et al., 2022; Calabrese et al., 2022); and with recent international emphasis on CDR for climate change mitigation there has been a proliferation in experimental and modeling studies seeking to verify and improve quantification of ERW's underlying mechanisms (e.g., Vanderkloot and Ryan, 2023; Beerling et al., 2018; Guo et al., 2023; Deng et al., 2023; Knapp et al., 2023; Kanzaki et al., 2023; te Pas et al., 2023; Reershemius et al., 2023; Reynaert et al., 2023; Chen et al., 2023; Paessler et al., 2023; Gaucher et al., 2023).

Based on a review of the literature, the IPCC estimates that the global CDR potential for ERW ranges from 2 to 4 Gt CO_2 yr^{-1} (IPCC, 2022a,b; Table TS.7). For comparison, the rate of CO_2 consumption by natural silicate weathering processes (the global rock weathering carbon sink) is estimated to be around 0.13 Gt CO_2 yr^{-1} (Zhang et al., 2021). The anthropogenic emissions from agriculture, forestry, and other land use are 5.9 $\pm$ 4.1 Gt CO_2 yr^{-1} (IPCC, 2022a,b; Table TS.4). Therefore, the global application of ERW has the potential to offset a large proportion of anthropogenic emissions from land use. In addition to CO_2 drawdown, the addition of silicate rocks such as basalt has been shown to reduce soil emissions of nitrous oxide (a potent greenhouse gas associated with agricultural processes) by up to 32%, depending on crop type (Blanc-Betes et al., 2021; Chiaravalloti et al., 2023, Beerling et al., 2018).

The use of silicate rock powders as slow-release fertilizers (commonly referred to as soil remineralizers) has been practiced and studied systematically since the 19th century (e.g., Hensel, 1894). For the past few decades, the study of soil remineralization with rock powders has played an important role in promoting the transition away from agricultural methods based on synthetic fertilizers to more sustainable, regenerative farming practices based on locally-sourced organic inputs and remineralizers (Chesworth et al., 1983; Leonardos et al., 2000; Theodoro and Leonardos, 2006; Fyfe et al., 2006; van Straaten, 2006; Campe, 2014; Manning and Theodoro, 2020; Theodoro et al., 2021; Conceição et al., 2022; Ramos et al., 2022; van Straaten, 2022; Campe et al., 2022; Swoboda et al., 2022).

The sustainability and success of an ERW or soil remineralization ultimately depend on two categories of variables: (1) biogeochemical factors that determine rock weathering rates and (2) life-cycle factors that determine the potential for environmental damage and the extent of carbon emissions resulting from rock extraction, crushing and transport. This paper presents a reduced-order systems model for ERW that accounts for biogeochemical and life-cycle variables. The model focuses on one aspect of ERW life cycle assessment: net carbon dioxide balance. Other life cycle assessment considerations are identified (e.g., the potential environmental and health risks of ERW), but these are not quantified in the new model. Specifically, this study aims to quantitatively explore how the dynamic relationships between variables such as rock mineralogy, soil pH, temperature, grain size, biological activity, and CO_2 emissions factors for rock processing and transport determine the net CO_2 emissions for a given ERW application. The model presented is a publicly available quantitative tool offering a systems-based approach for co-optimizing key variables for ERW applications.
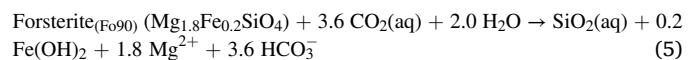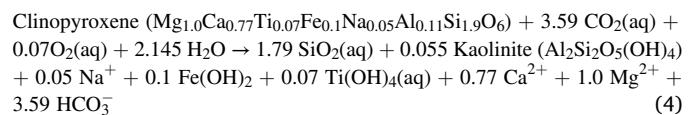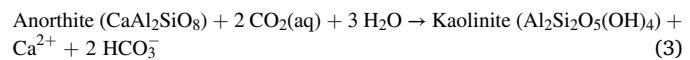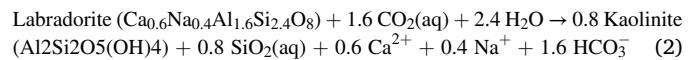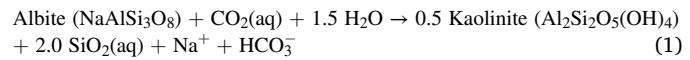
2. Theory and methods

2.1. The reaction pathways and capacity of carbon dioxide removal by enhanced rock weathering

The reaction pathways of ERW ultimately remove carbon dioxide by converting CO_2 to carbonate species. The process starts with the dissolution of atmospheric CO_2 in rainwater to form carbonic acid. This weak acid then attacks the silicate minerals that have been added to the soil. The resulting enhanced weathering reactions (as shown below) produce carbonate species that either precipitate or are transported to oceans, where they may counter ocean acidity (Taylor et al., 2016). The carbon converted from CO_2 to carbonates by these pathways remain in the geosphere (carbonate rocks), and the hydrosphere (ocean) sinks for thousands to millions of years (e.g., Zeebe and Wolf-Gladrow, 2009).

As mentioned above, silicate rock powders added to soils also act as slow-release fertilizers (remineralizers) that have been demonstrated to increase crop yield, thus increasing the plant biomass and the amount of soil organic carbon. This is another process by which ERW can remove CO_2 from the atmosphere; however, due to this effect's site-specific and plant-specific nature, it is generally not accounted for in generalized ERW process models such as the one presented in this paper.

The mass of CO_2 consumed by chemical weathering processes depends on the cationic flux (e.g., Ca^{2+}, Mg^{2+}, Na^+, and K^+) released from the dissolving minerals. This flux of positive charge is balanced by the formation of anionic carbonate species such as bicarbonate (HCO_3^-) or carbonate (CO_3^{2-}) at high pH. For this reason, minerals containing divalent cations convert more CO_2 to carbonate relative to monovalent cations (on a molar basis). This is evident in the mineral weathering reactions shown below.

$$\text{Albite (NaAlSi}_3\text{O}_8\text{)} + CO_2\text{(aq)} + 1.5\,H_2O \rightarrow 0.5 \text{ Kaolinite (Al}_2\text{Si}_2\text{O}_5\text{(OH)}_4\text{)} + 2.0 \text{ SiO}_2\text{(aq)} + Na^+ + HCO_3^- \tag{1}$$

$$\text{Labradorite (Ca}_{0.6}\text{Na}_{0.4}\text{Al}_{1.6}\text{Si}_{2.4}\text{O}_8\text{)} + 1.6\,CO_2\text{(aq)} + 2.4\,H_2O \rightarrow 0.8 \text{ Kaolinite (Al2Si2O5(OH)4)} + 0.8 \text{ SiO}_2\text{(aq)} + 0.6\,Ca^{2+} + 0.4\,Na^+ + 1.6\,HCO_3^- \tag{2}$$

$$\text{Anorthite (CaAl}_2\text{SiO}_8\text{)} + 2\,CO_2\text{(aq)} + 3\,H_2O \rightarrow \text{Kaolinite (Al}_2\text{Si}_2\text{O}_5\text{(OH)}_4\text{)} + Ca^{2+} + 2\,HCO_3^- \tag{3}$$

$$\text{Clinopyroxene (Mg}_{1.0}\text{Ca}_{0.77}\text{Ti}_{0.07}\text{Fe}_{0.1}\text{Na}_{0.05}\text{Al}_{0.11}\text{Si}_{1.9}\text{O}_6\text{)} + 3.59\,CO_2\text{(aq)} + 0.07\,O_2\text{(aq)} + 2.145\,H_2O \rightarrow 1.79 \text{ SiO}_2\text{(aq)} + 0.055 \text{ Kaolinite (Al}_2\text{Si}_2\text{O}_5\text{(OH)}_4\text{)} + 0.05\,Na^+ + 0.1\,\text{Fe(OH)}_2 + 0.07\,\text{Ti(OH)}_4\text{(aq)} + 0.77\,Ca^{2+} + 1.0\,Mg^{2+} + 3.59\,HCO_3^- \tag{4}$$

$$\text{Forsterite}_{(\text{Fo90})} \text{ (Mg}_{1.8}\text{Fe}_{0.2}\text{SiO}_4\text{)} + 3.6\,CO_2\text{(aq)} + 2.0\,H_2O \rightarrow \text{SiO}_2\text{(aq)} + 0.2\,\text{Fe(OH)}_2 + 1.8\,Mg^{2+} + 3.6\,HCO_3^- \tag{5}$$

The compositions for the clinopyroxene and forsterite (reactions 4 and 5) are based on mineral chemical analyses from basaltic samples by Koukouzas et al., 2019. Note that the molar ratio of CO_2 consumed to the reacting primary mineral increases for more calcium and magnesium-rich minerals. The accumulation of the potentially toxic metals nickel and chromium (reactions 4 and 5) are not included in the current version of our ERW model but could pose environmental hazards under some conditions and, therefore, should be accounted for when planning ERW field trials (see Suhrhoff, 2022; Vink and Knops, 2023; Dupla et al., 2023; Vink et al., 2022 for more details on the behavior of Ni and Cr in ERW applications).

The carbon dioxide drawdown capacity or enhanced weathering potential (EWP) for rocks, minerals, and alkaline industrial byproducts (e.g., ash and slag from steel production) can be quantified based on bulk oxide composition using a modified form of the Steinour equation (Steinour, 1959). The formulation of the EWP equation used in the current study is from Renforth, 2019, Bullock et al., 2021; Bullock et al., 2023. In these studies, the enhanced weathering potential of a material (with the units of kg CO_2 consumed per tonne of rock applied) is calculated as follows:

$$EWP = \frac{M_{CO_2}}{100}$$
$$\bullet \left(\alpha \frac{CaO}{M_{CaO}} + \beta \frac{MgO}{M_{MgO}} + \varepsilon \frac{Na_2O}{M_{Na_2O}} + \theta \frac{K_2O}{M_{K_2O}} + \rho \frac{MnO}{M_{MnO}} + \gamma \frac{SO_3}{M_{SO_3}} + \delta \frac{P_2O_5}{M_{P_2O_5}} \right)$$
$$\bullet 1000 \bullet \eta$$

(6)

Where CaO, MgO, Na_2O, K_2O, MnO, SO_3 and P_2O_5 quantify the oxide composition of the material (in weight percent), M_{oxide} are the molecular masses of the oxides, and α, β, ε, θ, ρ, γ, δ are coefficients that quantify the contribution of each oxide to the CO_2-consuming reactions (Renforth, 2019). Following Renforth, 2019; Bullock et al., 2021, α, β, ε, θ and ρ are set to 1.0 while $\gamma = -1.0$ and $\delta = -2.0$. Aluminum, iron, and titanium are not included in the EWP calculation because they are assumed to form secondary minerals in the soils (e.g., kaolinite and iron and titanium hydroxides, as shown in reactions 1–5).

The parameter η is the molar ratio of the CO_2 consumed to the divalent cations present in the reactions. Reactions (3) and (5) above imply η should have a value of 2; however, due to temperature effects, pCO_2-dependent carbonate speciation, and buffering in seawater, the parameter varies between 1.4 and 1.79 (Lefebvre et al., 2019). A default value of 1.5 is used for η in the present study. This value is deemed a conservative global average by Renforth, 2019. The importance of this parameter value in quantifying ERW CDR potential is covered in the model sensitivity analyses discussed in Section 3 below.

If carbonate minerals such as calcite or magnesite precipitate as a result of ERW reactions, some CO_2 is re-emitted, as shown in the reactions below:

$$Ca^{2+} + 2HCO_3^- \rightarrow CO_2 + H_2O + CaCO_3 \text{ (calcite)} \quad (7)$$

$$Mg^{2+} + 2HCO_3^- \rightarrow CO_2 + H_2O + MgCO_3 \text{ (magnesite)} \quad (8)$$

In addition to re-emitting some CO_2 these carbonation reactions "trap" or store carbon as solid precipitates that may remain stable for millions of years in the form of limestone.

However, because of the re-emission of CO_2, the carbonation pathways have lower overall CO_2 drawdown potential, as represented by a η value of 1.0 in equation (6) (e.g., Bullock et al., 2023).

A potential source of error in Equation (6) is that it assumes the ultimate fate of the bicarbonate produced during the rock powder weathering reactions is the Ocean. However, there will also be a considerable flux of ERW-produced bicarbonate to groundwater. It is also recognized that the chemical speciation of carbonate ions within groundwater may play a key role in determining the long-term efficiency of ERW as a CDR. We address this in the Stella ERW model by deriving a carbonate speciation function that modifies the EWP values calculated using the modified Steinour equation (Equation (6)). The carbonate speciation function is discussed in section 2.4.4 below, and in Section 2.9 of the Supplementary Information file.

2.2. Co-benefits and environmental risks of enhanced rock weathering

The IPCC 2022 climate mitigation report identifies several co-benefits of ERW, such as accentuated plant growth, reduced erosion, enhanced soil carbon accumulation, reduced soil acidity, and enhanced soil water retention. The benefits of using rock powders as soil amendments were recognized and studied well before ERW began to be investigated as a large-scale CDR strategy (e.g., Hensel, 1894); therefore, from an agricultural perspective, ERW's carbon dioxide removal potential can be considered a co-benefit of soil remineralization. It is, in fact, impossible to separate the ERW CDR effect from macro and microbiological rhizosphere processes as these phenomena play a dominant role in determining rock weathering rates (e.g., Schatz et al., 1954; Henderson and Duff, 1963; Boyle and Voigt, 1973; Banfield et al., 1999; Huang and Schnitzer, 1986; Banfield et al., 1999; Harley and Gilkes, 2000; Hoffland et al., 2004; Manning and Renforth 2013;

Zaharescu et al., 2020; Wild et al., 2022; Fang et al., 2023).

In addition to the classic soil remineralization research papers cited in Section 1., there have been many technical studies quantifying how rock powder amendments enhance soil properties and plant health (e.g., Gillman, 1980; Gillman et al., 2002, Sikora, 2004; Anda et al., 2009; Anda et al., 2015; Basak et al., 2017; de Aquino et al., 2020; Marchi et al., 2020; Busato et al., 2022; Krahl et al., 2022). Table 1 identifies ERW's demonstrated co-benefits and the associated UN sustainability goals they address.

Another important finding pertaining to the safety of ERW is the study of Gastmans et al., 2016. These researchers show that the basaltic Serra Geral Aquifer (Northeastern São Paulo state, Brazil) is a source of safe drinking water for millions of people. The groundwater in this large basalt deposit is rich in calcium, magnesium, and bicarbonate, with pH values ranging from neutral to alkaline. The weathering of the magnesium and calcium-rich aquifer minerals consumes carbon dioxide, converting it to bicarbonate in the process. This study was not explicitly investigating ERW; however, it provides reassurance that applying basaltic rock dust (of the type found in Northern São Paulo state) to

Table 1

Benefits of using rock powders as agricultural soil amendments (many of the benefits listed are adapted from Smith et al., 2019).

Demonstrated benefits	United Nations sustainability goals
▪ Removes carbon dioxide from the atmosphere and converts it to geologically stable carbonates.	Climate Action (SDG 13)
▪ Reduces the need for synthetic fertilizers, which have a high carbon footprint due to the energy needed for production and emissions from fertilized soils.	
▪ Counteracts soil acidity, significantly decreasing nitrous oxide emissions from composts and soils.	
▪ Improves crop yield and nutrient density.	Zero Hunger (SDG 2)
▪ Provides growth-limiting nutrients and essential trace elements for crop plants.	
▪ Counteracts soil acidification.	
▪ Provides plant-available silica, which enhances plant resistance to pests and disease.	
▪ Improves cation-exchange capacity (enhances long-term fertility).	
▪ Counteracts soil degradation and erosion.	
▪ Counteracts ocean acidification (mitigating harmful impacts on corals and fisheries) by enriching runoff and streams with bicarbonate and carbonate ions.	Life Below Water (SDG 14)
▪ Increased silica concentrations in runoff into water bodies favor the growth of diatoms over harmful non-siliceous algae (helping prevent algal blooms and resultant aquatic oxygen depletion).	
▪ Decreases the need for agrochemicals, thus reducing the consumption of pesticides and synthetic fertilizers (ammonium, potassium, nitrate, and phosphate).	Responsible Consumption and Production (SDG 12)
▪ Supports sustainable, regenerative agriculture as the rock powders used for ERW are usually locally sourced materials.	
▪ Counteracts soil degradation and increases the productivity of agricultural lands, thus minimizing the demand for expanding croplands. This mitigates the impacts on biodiversity caused by the conversion of natural areas into farmland.	Life On Land (SDG 15)
▪ There is anecdotal evidence from farmers that biodiversity improves when natural rock powders are substituted for synthetic fertilizers; however, no peer-reviewed studies were found documenting this observation.	

agricultural soils will not contaminate local surface and groundwaters.

For a thorough review of results from field and pot tests investigating how silicate rock powder applications affect soil properties and plant growth, see Swoboda et al., 2022.

As with any large-scale environmental intervention, ERW has potential risks for harmful ecological and human impacts (e.g., see Choi et al., 2021). The IPCC, 2022a,b (Table TS.7) identifies mining and air quality impacts as potential risks for ERW. Table 2 below identifies several more potentially harmful outcomes associated with poorly planned and poorly managed ERW applications.

Table 2
Potential ecological and human impact risks of ERW (largely adapted from Edwards et al., 2017; Klemme et al., 2022).

Potential risks and harmful impacts of enhanced rock weathering	Life cycle impact categories
■ It is unknown how wildlife in forest, river, and lake environments adjacent to ERW fields will respond to changes in pH and silicate particulate loads in the runoff.	Eco-toxicity
■ Increased inorganic turbidity and sedimentation in water bodies that receive excess silicate powders from runoff. This could negatively affect fish populations (Kemp et al., 2011) and coral health, diversity, and depth limit (Fabricius, 2005).	Eco-toxicity
■ Large doses of silicate rock type could cause toxic metal accumulation (e.g., Cr and Ni) in soils and potential plant uptake (Haque et al., 2020; Kierczak et al., 2021 for example, found that soils derived from ultramafic silicate rocks (i.e., rocks mainly consisting of olivine or serpentine) from over 20 different countries contained Ni and Cr concentrations well over the median world regulatory guidance values for these elements. However, it should be noted that there is no evidence of toxic metal accumulation from ERW field experiments using basaltic rock powders.	Eco-toxicity
■ Large-scale ERW would require an expansion of silicate mining operations. Mine creation causes significant environmental destruction and possible deforestation in tropical regions. The need for road and rail infrastructure associated with mining also may have negative environmental impacts.	Land use, Depletion of abiotic resources
■ Working with rock powders that contain crystalline silica poses a significant risk to human health through silicosis and other respiratory diseases. There is a potential risk of ingestion during rock crushing, milling, and spreading. This risk can be mitigated by using rock types that do not contain crystalline silica and ensuring that the rock dust is not contaminated with silica during crushing.	Particulate matter emissions, Human toxicity
■ Increasing the pH in tropical peatlands may cause significant environmental damage. For example, from Klemme et al., 2022: "Our findings suggest that in contrast to the desired impact, enhanced weathering may destabilize the natural carbon cycle in tropical peatlands that act as important carbon sinks and protect against coastal erosion."	Climate change
■ Long transport distances and high electric energy emissions factors for rock crushing and milling can limit the net carbon drawdown with the possibility of net positive emissions if rock types with low enhanced weathering potential and slow weathering rates are used. However, it should be noted that the emissions from crushing depend on the energy mix and not all crushing is energy intensive.	Climate change

It is important to note that it cannot be assumed that the risks listed in Table 2 apply equally in every ERW application scenario. In fact, it is highly unlikely that they will. In Brazil, a world leader in using natural rock powders for soil remineralization, the chemical risk associated with rock dust application to agricultural soils is managed by law (e.g., Brazil, 2013). Given the significant benefits and risks of ERW, it is essential that the main biogeochemical and life-cycle variables are co-optimized while planning and implementing large-scale ERW projects. This paper presents a modeling approach that accounts for the major variables in a systems format. The results discussed below focus specifically on the climate change impact categories identified in Table 2.

2.3. Model description

The enhanced rock weathering model discussed in this study was developed using the system dynamics modeling code Stella Architect (by isee systems). The code is an object-oriented programming environment that produces finite difference equations solved by user-selected, standard numerical methods such as the Euler method or Runge-Kutta methods (2nd or 4th order). We chose Stella Architect over standard life cycle assessment codes because if offers the flexibility to include the dynamics of mineral dissolution kinetics as a function of multiple variables that may change with time (e.g., pH and mineral surface area). The processes quantified in the model are shown pictorially in Fig. 1, and a simplified version of the model stock and flow diagram is shown in Fig. 2. The model will be referred to as the Stella ERW model in this paper.

Figs. 1 and 2 show that, in addition to accounting for CDR by rock weathering, the Stella ERW model accounts for CO_2 emissions from rock extraction, rock loading, transportation, crushing, milling, and spreading. The specific processes and parameter values used to quantify CO_2 emissions associated with ERW applications are presented in Section S1 and Tables S1–S4 of the Supplementary Information. The majority of parameter values and error ranges used are from Lefebvre et al., 2019. To account for the variability in CO_2 emissions from rock transport, the emissions factors from five-rock hauler truck types are considered in the model (see Table S3). These values also come from the ERW life-cycle analyses of Lefebvre et al., 2019. The transportation distance between the mine/quarry and the crushing/milling facility is assumed to be 1 km for all model runs presented. The average distance between the crushing/milling facility and the field is varied from 5 to 600 km.

The rock comminution operation for the Stella ERW model is also assumed to be the same as that used in the Lefebvre et al., 2019 life cycle study. Section S1.3 and Table S4 of the Supplementary Information discusses the process stages, emission factors, and associated uncertainties with rock crushing. The amount of electrical energy required to mill the rock to sub-millimeter grain sizes is calculated using the Bond equation (Bond, 1952), which is also discussed in Section S1.3 (see Equation S1 and Table S5). The CO_2 emissions from rock milling are calculated based on the electricity emissions factors, which depend on the regional energy mix, as discussed in Section 1.3 (see Tables S6–S8). The variation in emissions from rock comminution is accounted for in the model sensitivity analyses (Section 3 below) by varying the electric energy mixture. The current model version accounts for electric energy mixtures for Brazil, India, the US, and a no-fossil-fuel case.

2.4. Rock weathering sub-model

Three model rock types were formulated for this study with the purpose of spanning relevant ranges of rock compositions, dissolution rates, and enhanced weathering potentials. To define the rock compositions, a suite of model minerals was formulated based loosely on mineral chemical data from Lewis et al., 2021, Koukouzas et al., 2019, de Aquino et al., 2020. Details of the model mineral and rock compositions and their enhanced weathering potentials (calculated using

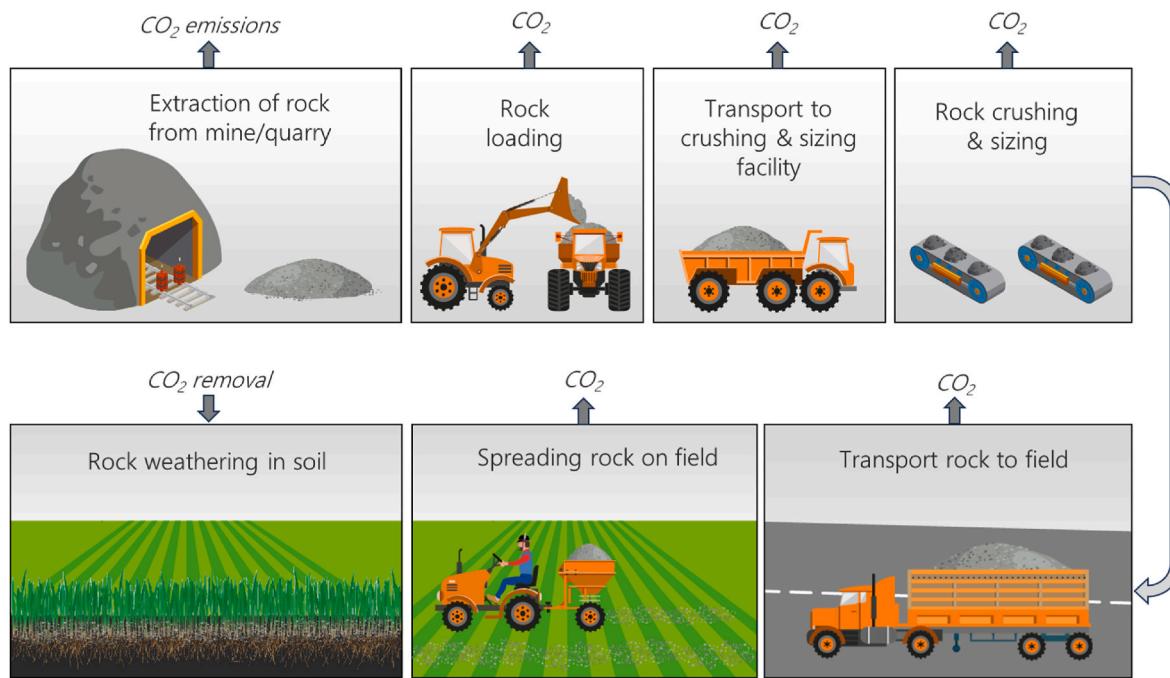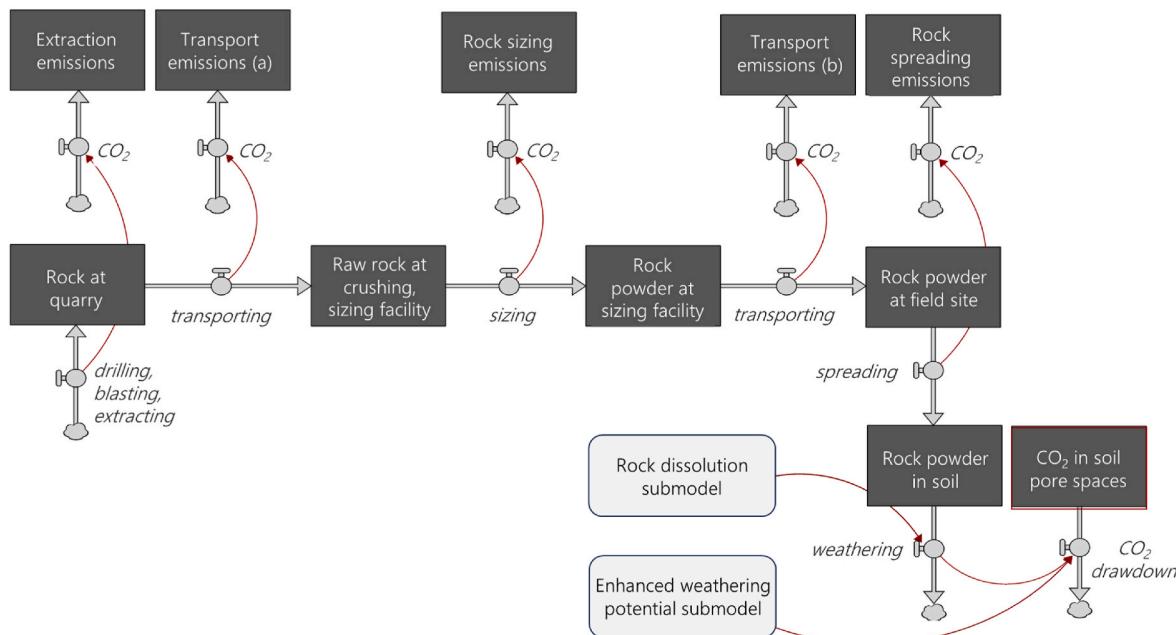**Fig. 1.** Processes quantified in the Stella ERW model.

Fig. 2. Simplified stock and flow diagram showing the layout of the Stella ERW model.

Equation (6)) are presented in Tables S9–S11 (Supplementary Information) and summarized in Table 3 below.

The total alkalis vs. silica classification of the basalt and basaltic andesite are shown in Fig. S1 of the Supplementary Information.

2.4.1. Abiotic weathering rates

The bulk dissolution rates of the model rocks are calculated using the Palandri and Kharaka (2004) formulations of the standard Transition State Theory kinetic rate laws for mineral dissolution. The resulting rock dissolution rates as a function of pH were compared to experimental data to verify accuracy and provide a measure of rate constant uncertainty (see Fig. S2 and Table S10, Supplementally Information).

The initial three model rocks used in the Stella ERW model (others can be added by users) were formulated to provide a range of dissolution rates as a function of pH, as shown in Fig. 3. As shown in Fig. 3a, basalt and basaltic andesite follow "V-shaped" dissolution patterns typical of basalt (e.g., Brantley, 2008, Fig. 5.1, Gudbrandsson et al., 2011; Pollyea and Rimstidt, 2017). The shape of this dissolution pattern, which has important real-world consequences for ERW applications, reflects the chemical weathering behavior of the rock's constituent minerals. As shown in Fig. 3b, plagioclase, basaltic glass, and potassium feldspars all display V-shaped dissolution curves. In the absence of experimental kinetic data for a particular rock type, its dissolution behavior may be estimated using the weighted sums of the dissolution rates of its

Table 3
Mineralogy and enhanced weathering potential of model rocks.

Model rock type	Enhanced weathering potential[a] (kg CO_2 t^{-1} rock)	Minerals (mass %)
Dunite	795	▪ 96% Forsterite (Fo90) ▪ 2% Augite ▪ 2% Enstatite
Basalt (*olivine basalt*)	401	▪ 40% Labradorite ▪ 24% Augite ▪ 20% Forsterite ▪ 10% Glass ▪ <5% Sanidine, Apatite
Basaltic Andesite	226	▪ 65% Labradorite ▪ 10% Glass ▪ 10% Enstatite ▪ 10% Sanidine ▪ <5% Augite, Apatite

[a] Calculated using Equation (6).

constituent minerals (Pollyea and Rimstidt, 2017). This was done for the model rocks used in the Stella ERW model, as shown in Fig. 3b. This method is shown to be reasonably accurate by the observation that the Stella ERW model rock dissolution rates closely match experimental data for similar lithologies (see Fig. S2).

The rate equations used to calculate mineral and rock weathering rates are shown as Equations (10)–(12) below. The formulations of these equations and most of the rate parameters used are from Palandri and Kharaka (2004).

For dissolution under acidic conditions, the equation is as follows;

$$\frac{dm}{dt} = - SA \left[k_{acid}^{298.15K} \, exp \left(\frac{-E_{acid}}{R} \left(\frac{1}{T} - \frac{1}{298.15K} \right) \right) a_{H^+}^{n_1} (1 - \Omega^{p_1})^{q_1} \right] \quad (10)$$

Under neutral conditions:

$$\frac{dm}{dt} = - SA \left[k_{neutral}^{298.15K} \, exp \left(\frac{-E_{neutral}}{R} \left(\frac{1}{T} - \frac{1}{298.15K} \right) \right) (1 - \Omega^{p_2})^{q_2} \right] \quad (11)$$

And for basic conditions:

$$\frac{dm}{dt} = - SA \left[k_{base}^{298.15K} \, exp \left(\frac{-E_{base}}{R} \left(\frac{1}{T} - \frac{1}{298.15K} \right) \right) a_{H^+}^{n_3} (1 - \Omega^{p_3})^{q_3} \right] \quad (12)$$

Where $\frac{dm}{dt}$ is the dissolution rate in mols per second, *SA* is the mineral or rock surface area in m^2, *E* is the activation energy (Joules per mole) which quantifies the temperature dependence, *R* is the universal gas constant, *T* is absolute temperature, a_{H^+} is the activity of hydrogen ion, *n* is the reaction order with respect to hydrogen ion, and Ω is the saturation index, which quantifies the mineral saturation state of the soil pore water ($\Omega = \frac{Q}{K}$ where *Q* is the ion activity product, and *K* is the equilibrium constant). The exponents p_i and q_i are empirical, dimensionless parameters that describe specific reaction mechanisms. These exponents are only known for a few minerals. The default values for both of these parameters in the Stella ERW model are 1.0.

The rate constant, activation energies, and reaction order parameters for individual minerals were taken from the compilation of Palandri and Kharaka (2004), except for the basic mechanism parameters for labradorite and sanidine, which come from Heřmanská et al., 2022. The surface area, temperature, hydrogen ion activity (pH), and saturation index are all model variables that account for variations in soil conditions. The dissolution rate equation and parameter values for the basaltic glass phase, which makes up 10% of both the basalt and basaltic andesite model rocks, were taken from Pollyea and Rimstidt, 2017. Note that the Stella ERW model is not a reactive transport model or reaction path model. The Stella ERW model carries out mass balance and dissolution kinetic calculations to determine the net CDR for a given ERW scenario without using complicated mass transport or activity coefficient models.

For the scenarios modeled for this study, it is assumed that precipitation levels (i.e., water flux through the soils) do not limit the rock powder weathering rates. The Stella ERW model could indirectly simulate low water flux conditions by varying the saturation index parameter in the rock dissolution rate laws. In low flux conditions, the silica concentration of the soil pore waters would increase (as weathering continues in the stagnant moisture pockets), thus increasing the saturation index with respect to the primary silicate minerals. As shown in the model results below, once the saturation index exceeds 0.5, this process inhibits dissolution kinetics (i.e., slows chemical weathering rates). This is referred to as the chemical affinity effect and has been observed in field and laboratory studies of silicate mineral weathering (e.g., Drever and Stillings, 1997; White et al., 2001; Maher et al., 2009; White and Buss, 2014).

It is noted that the acidic mechanism can occur at higher soil pH in circumstances where biologically mediated protonation occurs. This
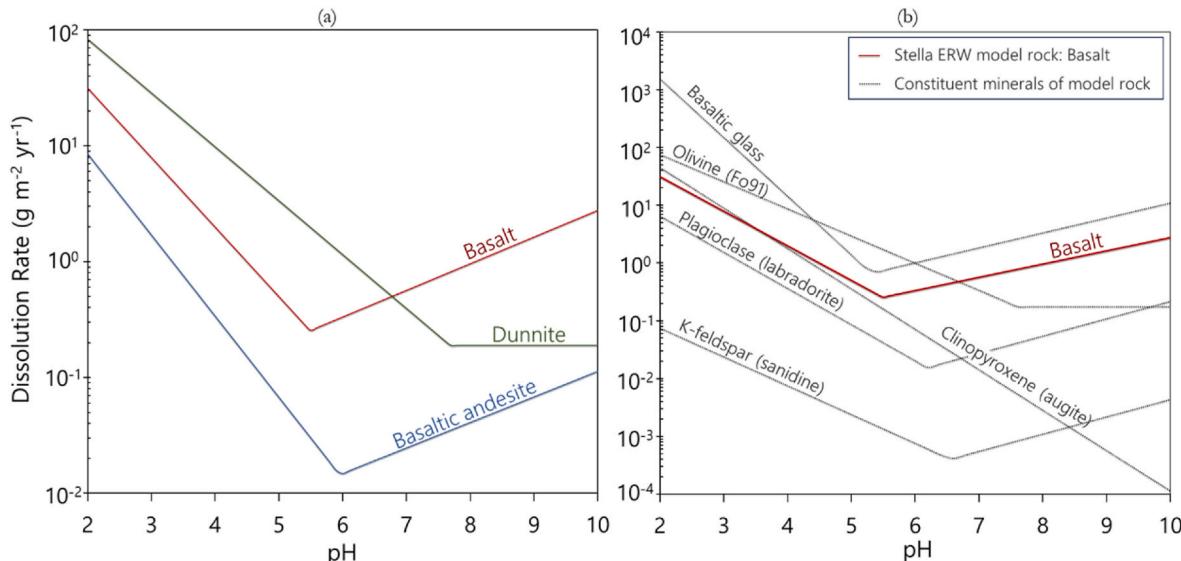

Fig. 3. Rock dissolution rates: (a) shows the pH dependence of the dissolution rates of the three model rocks, and (b) shows the pH dependence of the dissolution of constituent minerals of the basaltic model rock.

process is not explicitly accounted for in the present model; however, the biological function (from Beerling et al., 2020), which increases mineral dissolution rates, does provide a non-mechanistic method accounting for the role of biology in the mineral dissolution kinetics.

2.4.2. Biological influences on weathering rates

The influence of macro and microbiological processes on mineral weathering rates has been studied for decades (e.g., Schatz et al., 1954; Henderson and Duff, 1963; Boyle and Voigt, 1973; Banfield et al., 1999; Huang and Schnitzer, 1986; Banfield et al., 1999; Harley and Gilkes, 2000; Hoffland et al., 2004; Verbruggen et al., 2021; Manning and Renforth 2013; Zaharescu et al., 2020; Wild et al., 2022; Fang et al., 2023).

In the Stella ERW model, biological effects on rock weathering rates are accounted for using the biological function derived by Beerling et al., 2020. This function is an empirical fit to experimental weathering data from mesocosm experiments. These tests investigated basalt weathering rates for pots containing either annual or woody crops, and the role of mycorrhizal fungi was also quantified (Akter and Akagi, 2005, 2010; Quirk et al., 2012, 2014). The biological function derived from these tests captures the effects of plant biology and rhizosphere processes. These processes, such as the bond-breaking action of mycorrhizal fungi at mineral surfaces and the chelating action of root exudates, have been shown to accelerate mineral weathering significantly (Beerling et al., 2020, references cited above).

The use of the biological function in the mineral dissolution equation is shown in Equation (13), and its formulation is shown in Equation (14):

$$\frac{dm}{dt} = -SA\left[k_i^{298.15K}\,exp\left(\frac{-E_i}{R}\left(\frac{1}{T}-\frac{1}{298.15K}\right)\right)a_{H^+}^{n_3}(1-\Omega^{p_3})^{q_3}\right] \times f(NPP) \tag{13}$$

$$f(NPP) = a(x_{normalized} \times NPP_{normalized})^b + 1 \tag{14}$$

Where $NPP_{normalized}$ (abbreviated as NPP_n) is the normalized net primary production of the crop plant, and a, $x_{normalized}$, and b are fitted parameters (see Beerling et al., 2020, Supplementary Information Section 2.0). The biological function in the Stella ERW model is parameterized using the values reported by Beerling et al., 2020, Supplementary Information Table S5).

2.4.3. Grain size distributions and rock weathering rate calculations

The Stella ERW model uses a Gaussian grain size distribution based on a user-specified P80 particle size. The P80 variable is defined as the sieve mesh size (in micrometers) that passes 80% of the rock material in question and is the primary variable in the Bond equation discussed above (see Section S1.3 of the Supplementary Information). For example, a P80 of 100 μm means that 80% of the rock powder consists of grains smaller than 100 μm in diameter.

In the Stella ERW model, the range of grain sizes present for a given run consists of two normal distributions: one for the 80% of particles that are smaller than P80 and another one for the 20% of particles that are greater than P80 (i.e., did not pass the P80 sieve size). A more detailed discussion of how the different grain size fractions are treated in the model is given in Section S2.3 and Figs. S3 and S4, Supplementary Information.

Each grain size fraction's specific surface area (m²/g) is assumed to remain constant with time, where the specific surface area of each grain size fraction is determined using the Sauter equation (see Section S2.4, Supplemental Information). The Sauter equation yields a geometric surface area assuming spherical grains. This underestimates the actual mineral surface area (i.e., the reactive surface area). Thus, to improve the accuracy of estimations of this key variable, the surface area results from the Sauter equation are multiplied by a surface roughness factor. This factor, which accounts for grain surface irregularities and porosity, is determined using the method of Beerling et al., 2020 (see

Supplementary Information Section S2.4 of the present paper). The Stella ERW model does not employ a shrinking core mechanism to account for the evolving reactive surface area as used by Rinder and von Hagke, 2021) in their basalt dissolution model. Interestingly, Rinder and von Hagke (2021) show that their modified shrinking core model produces results similar to the steady state model of Strefler et al., 2018 for the first 10–20 years of comparable model runs. Therefore, the steady-state assumption (i.e., using constant specific surface areas for each grain size fraction) does not appear to add significant uncertainties for relatively short-term model runs (such as those presented in this paper).

2.4.4. Carbon dioxide removal calculation and carbonate speciation

The amount of rock weathered is multiplied by rock-specific EWP (Equation (6)) to determine the amount of CO_2 captured for every model time step. As shown in Equation (6), the EWP of a given rock type is dependent on its bulk composition (i.e., higher levels of divalent cations result in higher EWP). The EWP for the rock types currently included in the model ranges from 226 to 795 kg CO_2 t^{-1} of rock (Table 3). The Stella ERW model also accounts for carbonate speciation in determining the EWP. Under acidic conditions (pH values less than 6), carbonate ions are less thermodynamically stable than dissolved CO_2 (carbonic acid). Under these conditions, the EWP for a given rock powder will be lower than its theoretical value because carbonate alkalinity production ($HCO_3^- + CO_3^{2-}$) is thermodynamically restricted. This is accounted for in the Stella EWP model by multiplying the theoretical EWP by the fraction of carbonate alkalinity that is stable (which changes with pH during a given model run). The carbonate speciation calculation used to determine the carbonate alkalinity stability fraction is discussed in Section 2.9 of the Supplementary Information file.

2.4.5. pH evolution during model runs

As implied by Fig. 3 (and discussed further in Section 3 below), soil pH is a dominant variable in the model due to its strong influence on rock dissolution rates. Many of the experimental ERW and remineralization studies cited above observe increases in pH with time as alkalinity (mainly bicarbonate) is produced during rock weathering (see Equations (1)–(5)). The Stella ERW accounts for this effect using an empirical factor that scales pH to the mass of weathered rock with each time step. The factor is derived from the results of Shamshuddin et al., 2015, Fig. 1. Plots showing how pH evolves with time for four representative model cases are shown in Fig. S5, Supplementary Information.

2.4.6. Model scope, limitations, and uncertainty

"All models are wrong, but some are useful."
Box, 1979.

The Stella ERW model was developed to estimate the CDR potential and net CO_2 balance for a user-defined ERW application while accounting for variations in several major biogeochemical and life cycle variables. It is a reduced-order model developed with the philosophy of implementing the minimal number of processes needed to provide useful predictive assessments. Therefore, site-specific factors and detailed geobiological reaction mechanisms are not explicitly modeled.

The model's only dimension is time, and it does not include explicit pedologic, hydrologic, or agronomic simulations. It also lacks explicit treatments of climatological and biological processes such as precipitation patterns, plant growth, and organic matter accumulation. The model is, therefore, not meant to provide detailed information on the chemical evolution of soils during rock weathering. Nor does it provide information on crop yield, biomass accumulation, or variations in soil organic carbon. It, therefore, does not account for the biological storage of carbon in soils and plants, which is heavily dependent on site-specific conditions that the Stella ERW is not currently formulated to simulate. Rather, the appropriate use of the model is for scoping assessments of how variations in primary variables such as rock bulk chemistry, application rate, soil pH, grain size, transport distances, and energy use

emission factors impact the net CO_2 balance of a specific ERW application.

Model uncertainty runs were performed using the parameter error ranges provided in Tables S1, S2, and S4. Each uncertainty range was sampled at each time step over hundreds of model iterations (uncertainty distributions were adapted from Lefebvre et al., 2019). The results indicate that the uncertainty introduced by parameter error ranges is inconsequential in light of the uncertainties introduced by adjustable parameters such as the rock dissolution rate constants and EWP coefficient η (see Supplementary Information Section S2.6 and Fig. S6).

3. Results and discussion

Results from the Stella ERW model were compared to experimental data from ERW laboratory, mesocosm, and field studies to assess the model's accuracy. Results from the selected ERW studies are summarized in Table 5, and comparative plots are shown in Fig. 4. The model was then used to perform a series of sensitivity tests quantifying how variations in biogeochemical and rock processing life-cycle variables impact the net CO_2 balance for hypothetical ERW applications. The variables considered in this study, along with their default or base-case values, are given in Table 5.

In addition to the detailed results of the experimental studies shown in Table 4, the following overall CDR ranges are reported for basalt.

- 2 to 4 t CO_2 ha^{-1} over 1–5 years (Kelland et al., 2020)
- 1.3 to 8.5 t CO_2 ha^{-1} over 15 years (Lewis et al., 2021)
- 1.83 to 4.48 t CO_2 ha^{-1} over 1–5 years (Vienne et al., 2022)
- 3 to 7 t CO_2 ha^{-1} yr^{-1} (Vanderkloot and Ryan, 2023)
- 10.5 ± 3.8 t CO_2 ha^{-1} over 4 years (Beerling et al., 2024)
- 0.596 to 5.8 t CO_2 ha^{-1} over eight months (Paessler et al., 2023, preliminary results)

The measured CO_2 removal rates reported in the ERW studies highlighted above and in Table 4 range from less than 1 to around 7 t CO_2 ha^{-1} yr^{-1} for both olivine-based rocks and basalts (depending on

Table 5
Primary user-defined variables of the Stella ERW model.

Variable	Units	Default value	Modeled range[a]
Rock type	–	Basalt	Dunite, Basalt, Basaltic andesite
Rock application rate	Tonnes (t) ha^{-1}	10	1–50
Acidity	pH	5.0	3–9
Grain size (P80)	Micrometers	100	1–5000
Soil temperature	°C	25	5–50
Saturation index	unitless	1×10^{-9}	$1 \times 10^{-9} - 1.0$
Biological factor (NPP$_n$)	unitless	1.0	0–1.0
Enhanced weathering potential coefficient (η)	unitless	1.5	1.0–1.75
Distance from rock crushing/ milling facility to field	km	50	10–500
Emission factor for rock haulers	kg CO_2 t^{-1} km^{-1}	0.17	0.06–0.4
Emission factor for electricity production	kg CO_2 kWh^{-1}	0.4	0.03–0.8

[a] The range over which sensitivity tests were performed.

application rates and conditions). Results from the baseline Stella ERW model runs (discussed below) fall within this range.

Because of the differences in rock properties and conditions, it is not expected that the Stella ERW model would precisely reproduce the data from any of the studies shown in Table 4. However, as mentioned above, the model results are consistent with the overall experimental findings and, in some cases, closely match experimental observations. For example, model runs using the basalt model rock with application rates, grain sizes, and initial pH values corresponding to those of Kelland et al., 2020; Vienne et al., 2022 show good agreement with measured values (Fig. 4a). Performing the same model cases using the basaltic andesite model, rock underpredicted the experimental values by a factor of approximately 20. This is because of basaltic andesite's relatively slow dissolution rate under the specified conditions (i.e., a pH of 6.6 is close to the minimum in this rock type's dissolution curve; see Fig. 3). The pH

Table 4
Measured carbon dioxide removal rates from selected experiments.

Rock Type	Test type	Application rate (t ha^{-1})	CDR (t CO_2)	CDR duration (yr)	Grain size (micrometers)	pH (initial)[a]	Reference
Olivine	Pot	1.63	0.29	0.62	66% < 50	5	Berge et al., 2012
Olivine	Pot	204	2.69	0.62	66% < 50	5	Berge et al., 2012
Olivine	Pot	10	3.13[b]	0.25	50% < 20	4	Dietzen et al. (2018)
Olivine	Pot	50	4.16[b]	0.25	50% < 20	4	Dietzen et al. (2018)
Dunite	Mesocosm	220	0.02	1	80% < 1020	7	Amann et al., 2020
Dunite	Mesocosm	220	0.05	1	80% < 43.5	7	Amann et al., 2020
Basalt	Mesocosm	100	2.36[c]	1	80% < 1280	6.6	Kelland et al. (2020)
Basalt	Mesocosm	100	3.01	1	80% < 128	6.6	Kelland et al. (2020)
Basalt	Mesocosm	50	0.77	0.27	77% < 250	7.7[d]	Vienne et al. (2022)
Andesite	Field	50	~0.4	1	80% < 1767	4.2–6.4	Larkin et al. (2022)
Meta-basalt[e]	Field	50	3.8[f]	1	80% < 267	6.1	Beerling et al. (2024)
Meta-basalt[e]	Field	50	10.5	4	80% < 267	6.1	Beerling et al. (2024)
Basalt	Lysimeter	100	0.596–5.8[h]	0.67	80% < 850	~7	Paessler et al. (2023)
Basalt	Lysimeter	200	0.92–7.2[h]	0.67	80% < 850	~7	Paessler et al. (2023)
Basalt[g]	Column	50	6–7	1[i]	<45	3.4–4.2	Vanderkloot and Ryan (2023)
Basalt	Column	50	~4.5	1	45–150	3.4–4.2	Vanderkloot and Ryan (2023)
Basalt	Column	50	3–4	1	>150	3.4–4.2	Vanderkloot and Ryan (2023)

[a] Values are approximate; see references for pH variations during experiments.
[b] The measured drawdowns were 3.13 and 4.06 t CO_2 ha^{-1}, over 0.25 years.
[c] This study reports a range of 2–4 t CO_2 ha^{-1}, over 1–5 years for a single application of 100 t/ha.
[d] pH in soil pore water did not significantly change after basalt amendment.
[e] The rock used for this study was a metamorphosed basalt containing alteration minerals such as chlorite and actinolite.
[f] This study reports a CDR range of 3.8 t CO_2 ha^{-1}, in the first year to 10.5 t CO_2 ha^{-1} (time-integrated) after four annual rock powder applications.
[g] This study used both meta-basalt and basalt.
[h] Reported data are 0.596–5.8 and 0.920–7.2 t CO_2 ha^{-1} (for 100 and 200 t rock ha^{-1}, respectively) over eight months. The lower and higher values for each range were determined using independent techniques. Results are considered preliminary.
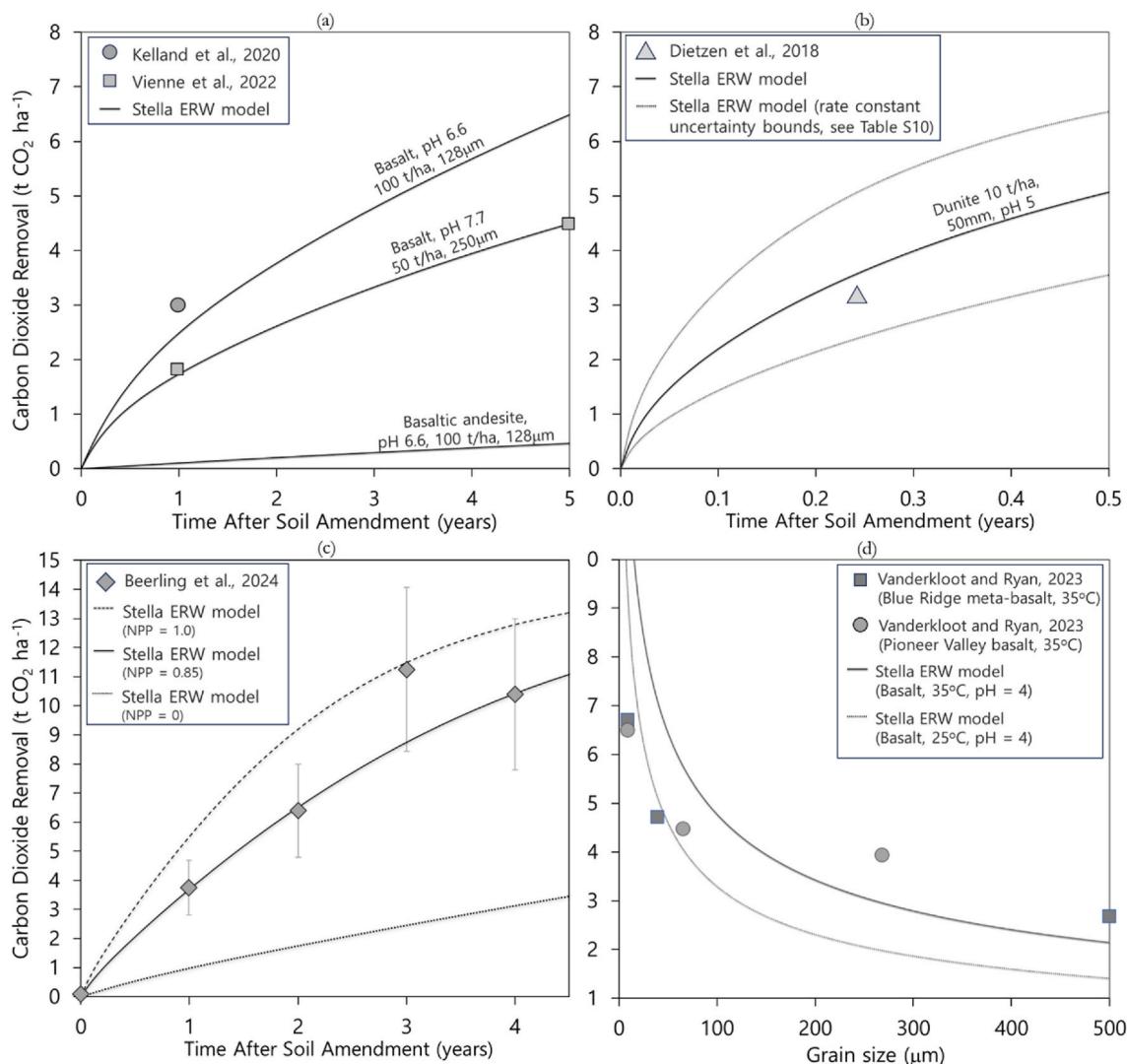[i] Actual experimental duration was 14 days; results were extrapolated to one year.

Fig. 4. Comparisons of Stella ERW model runs to selected experimental data. Plot (a) compares model runs for basalt to the data of Kelland et al., 2020; Vienne et al., 2022. Plot (b) compares model results for dunite to the data of Dietzen et al., 2018 (the dotted lines quantify the upper and lower uncertainty bounds for the rate constant). Plot (c) shows the model results compared to the data of Beerling et al., 2024. The error bars on the data points are for $\pm$ 25%. The data in this plot differs from others in that the rock application was repeated annually. The data points (and model runs) represent time-integrated CDR values. Plot (d) compares model results to the data of Vanderkloot and Ryan.

conditions noted in Fig. 4 are initial values. The pH increases with time during the model runs as rock powder dissolves; therefore, while bicarbonate production may be low early in the model scenarios (due to carbonate speciation, see Supplemental Information Section 2.9), it increases as soil acidity is neutralized during reaction progress.

Fig. 4b shows a model run for the dunite model rock with conditions roughly matching the experiment of Dietzen et al., 2018. Using the default parameters, the model slightly over-predicts the CDR for this scenario. This figure also shows the error envelope defined by the uncertainty in the dunite rate constant (see Table S10). Fig. 4c shows the time-integrated CDR results from the field study of Beerling et al., 2024. Using the default Stella ERW parameter settings and the basalt model rock, the model under-predicts the field results by a factor of approximatly 3. Altering the model to match the measured data requires increasing the basalt rate constant by a factor of 10 (or decreasing the model rock grain size from the experimental value of 267 μm down to 27 μm).

The Stella ERW model adequately reproduces the trends in data from the rock weathering studies of Vanderkloot and Ryan, 2023 (Fig. 4d). These data show an exponential increase in CDR with decreasing grain

size caused by the exponential rise in rock weathering rates. The model results follow the general trend of the data but slightly underpredict the experimental results at grain sizes less than 200 μm and over-predict the CDR for data at smaller grain sizes by a factor of approximately 2 (for the 35°C case). It should be noted that the Stella ERW model scenarios that were compared to the Vanderkloot and Ryan, 2023 data were run without the carbonate speciation function. It is likely that the CDR at the low pH values for these experiments would be considerably lower than reported due to the dominance of carbonic acid over bicarbonate and carbonate ions. See Section S2.9 of the Supplementary Information file.

Overall, the observations summarized in Fig. 4 lend confidence that the model accurately represents ERW phenomena, despite the limitations discussed in Section 2.4.6 above.

3.1. Biogeochemical variable sensitivity analyses

Fig. 5 shows results from a sensitivity analysis of the main model variables for the basalt model rock. The ordinate for each plot is the amount of carbon dioxide removed in tonnes CO_2 per hectare, which is determined by the rock's enhanced weathering potential (Equation (6))
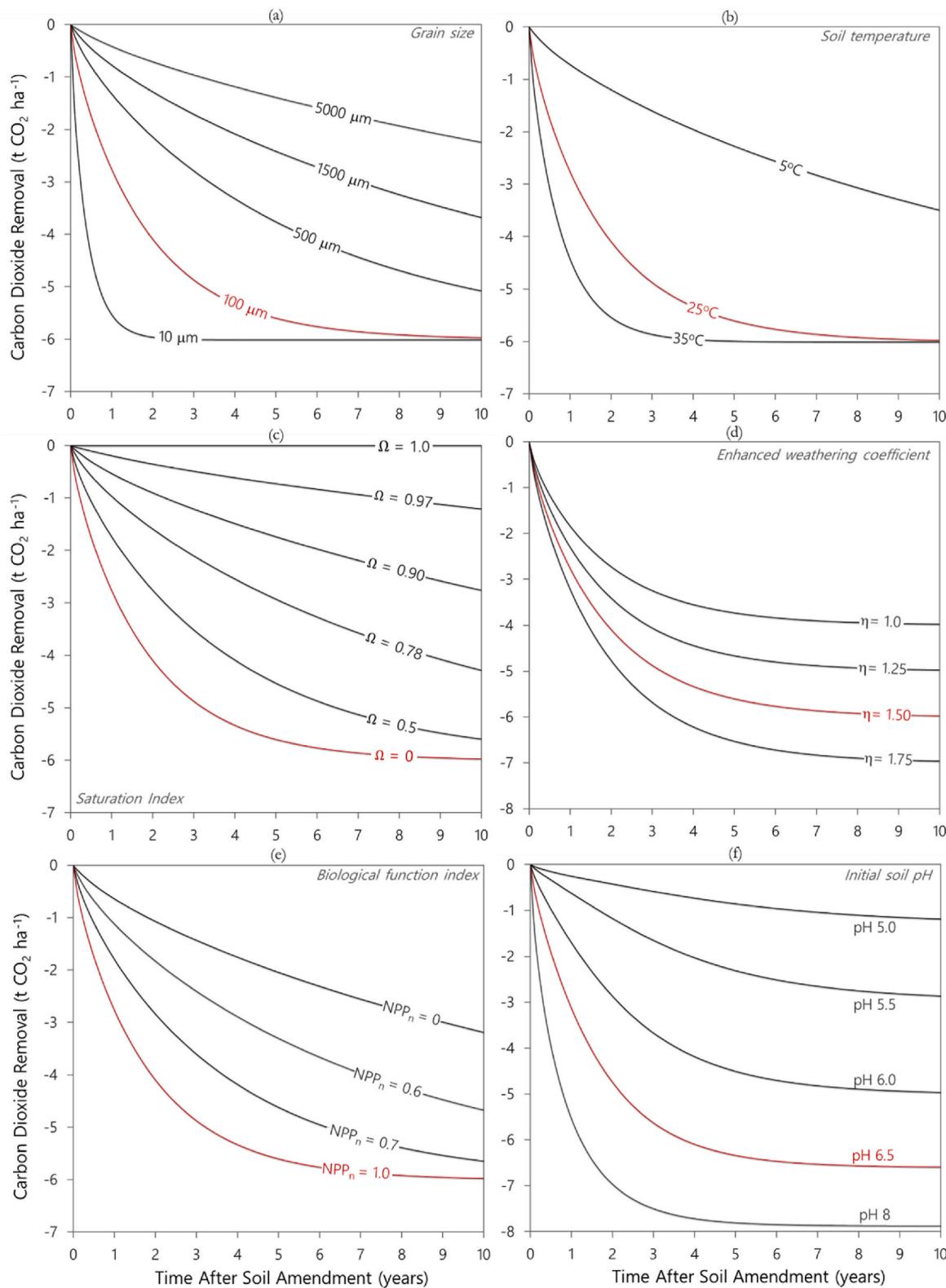
Fig. 5. Sensitivity analyses of how variations in key variables impact the predicted CDR for the basalt model rock. Panels (a), (b), (c), (d), (e), and (f) show results for grain size, soil temperature, saturation index (see Equation (6)), enhanced weathering coefficient (see Equation (11)), the biological function (see Equation (12)), and soil pH respectively.

multiplied by the mass of rock weathered (Equations (10)–(13)). The abscissa of each plot is the amount of time following the spreading of the rock powder onto the soil (an interval of 10 years was chosen). The curves highlighted in red are the values used for this sensitivity analysis

(i.e., the values of variables held constant for each run). Note that the plotted results are time-integrated, so they quantify the total mass of carbon dioxide removed (per hectare) at each point in time rather than an instantaneous rate of removal. A P80 grain size of 100 μm and an

initial pH of 6.5 were chosen to maximize the variation in results (i.e., show the full range of possible outcomes from complete rock weathering to minimal dissolution after ten years). The model cases shown in Fig. 5 do not include the transport and energy emissions life-cycle variables. Sensitivity runs that account for those variables are shown in Figs. 6 and

7 and are discussed below. Fig. 5a shows that the P80 grain size significantly influences the CDR capacity. For example, the 10 μm case reaches the EWP of the basalt model rock (around 6 t CO_2 ha^{-1}) around one year after application (i.e., nearly all of the rock is weathered), while the 5 mm case predicts a CDR of less than 2 t ha^{-1} at ten years. Note that
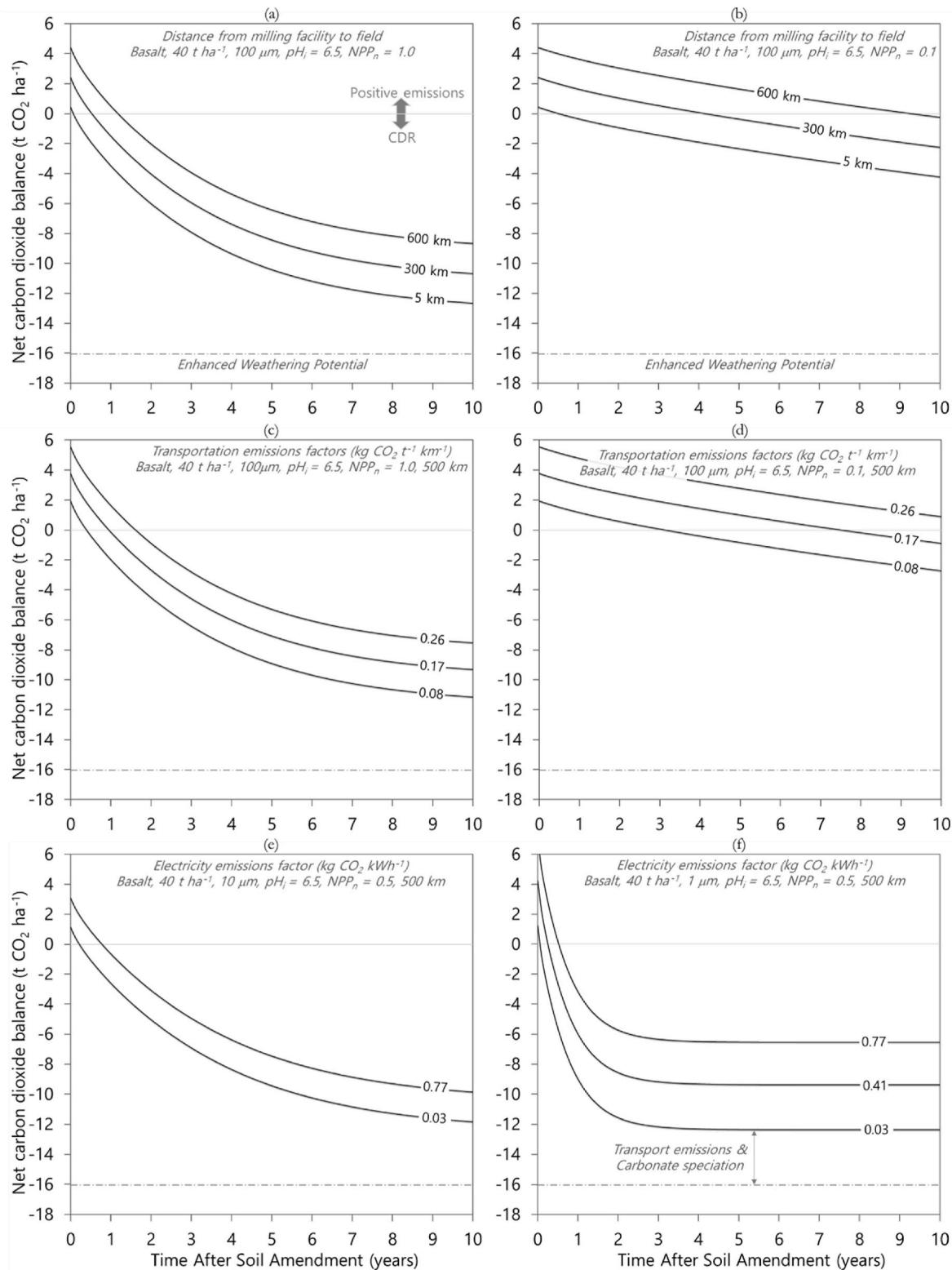

Fig. 6. Model runs showing how variations in life-cycle variables impact the CDR of the basalt model rock. The variables include: the distance between the rock milling facility and the field (a) and (b), the emission factors for rock haulers (c) and (d), and the emission factors for electrical power needed to mill the rock down to 10 μm (e) and 1 μm (f).

the EWP of the basalt rock represented in Fig. 5a–c (around 6 t CO$_2$ ha^{-1}) accounts for carbonate speciation (see Section 2.9 of the Supplementary Information file). Variations in soil temperature show that the system approaches the EWP within three years for the 35°C case and around eight years for the 25°C case. For a soil temperature of 5°C, the

model predicts a CDR of 3.5 t ha^{-1} at the 10-year mark (Fig. 5b).

The saturation index (Ω in Equations (10)–(13)) depends on the total dissolved solids (particularly SiO$_2$(aq)) in the soil solution and can significantly impact CDR capacity (Fig. 5c). For values less than 0.1, this parameter has little effect on weathering rates and, thus, little effect on
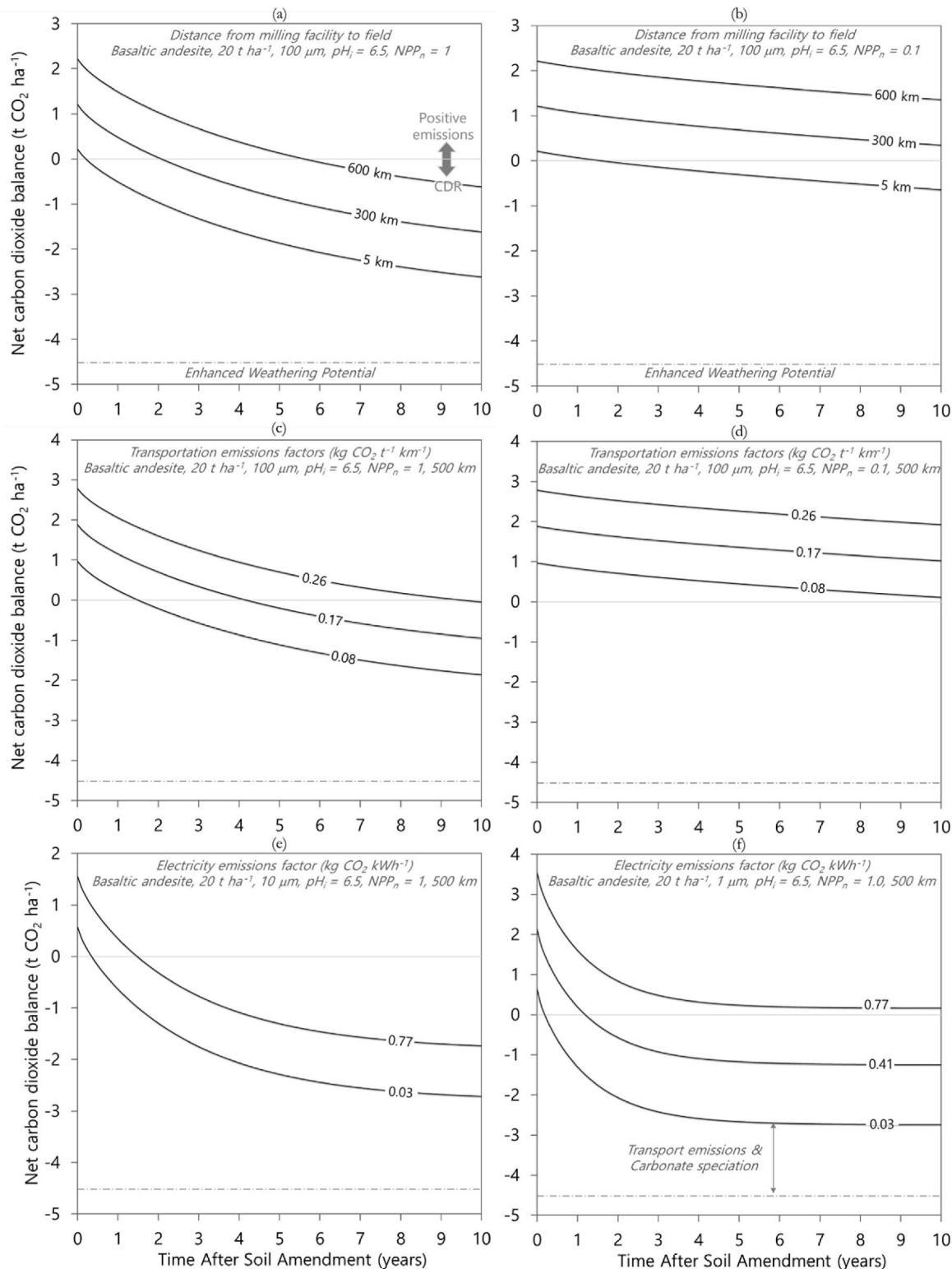

Fig. 7. Model runs showing how variations in life-cycle variables impact the CDR of the basaltic andesite model rock. The variables include: the distance between the rock milling facility and the field (a) and (b), the emission factors for rock haulers (c) and (d), and the emission factors for electrical power needed to mill the rock down to 10 μm (e) and 1 μm (f).

predicted CDR. However, it becomes significant at values greater than 0.5 (Fig. 5c). For example, a saturation index of below 0.1 results in a CDR of around 6 t ha^{-1} (after 10 years), while a Ω of 0.9 reduces the CDR to 2.8 t CO$_2$ ha^{-1}. Several processes determine the saturation index, including soil/rock mineralogy and hydrologic factors. The presence of low solubility silicate minerals coupled with long pore water residence times leads to high saturation index values.

The enhanced weathering coefficient η (Equation (6)) determines the maximum possible CDR for a given rock type. A value of 1.75 is near the maximum possible for this parameter and is predicted to result in an EWP of approximately 7 t CO$_2$ ha^{-1} (for olivine basalt, accounting for carbonate speciation). A value of 1.0 for η indicates the carbonation pathway (see Equations (7) and (8)), which yields an EWP of approximately 4 t CO$_2$ ha^{-1} (for olivine basalt, accounting for carbonate speciation). The maximum possible value for η is 2.0; however, this is unrealistic due to the inevitable conversion of carbonate alkalinity (specifically HCO$_3^-$) back to carbon dioxide downstream from the ERW application site.

The normalized net primary production index (NPP$_n$), which is used here to account for biological activity in the soil, also significantly impacts CDR capacity (Fig. 5e). As discussed in Section 2.4.2, NPP$_n$ is the independent variable in an empirical biological function (derived by Beerling et al., 2020) that modifies the rock weathering rate equations (Equation (13)). Low values of NPP$_n$ (i.e., low biological impacts on rock weathering rates) decrease CDR values by as much as 3 t CO$_2$ per hectare (Fig. 5e). The importance of NPP$_n$ is further highlighted in the life-cycle sensitivity analyses discussed in Section 3.3 below.

Fig. 5f shows that pH also plays a key role in the CDR capacity. The maximum CDR capacity for the example basalt model run shown in Fig. 5f is for a pH of 8. At this pH, there are no carbonate speciation effects (i.e., bicarbonate is at its maximum stability), thus the predicted CDR approaches the theoretical EWP of 8 t CO$_2$ ha^{-1}. The predicted CDR values decrease with decreasing pH due to carbonate speciation (See Section 2.9 of the Supplementary Information file). The pH also plays a key role in determining the dissolution rates of the minerals in the basalt. For basalts, the fastest weathering rates are realized under both acidic (i.e., around pH 5) and basic (i.e., around pH 8) conditions. This trend reflects the "v" shape of the basalt dissolution rate curve (Fig. 3) and highlights how knowledge of a rock's dissolution behavior as a function of pH can be used to optimize its application for ERW. However, the carbonate speciation effect cancels out CDR increases from fast mineral weathering rates at low pH (<6) because it lowers the effective EWP for the rock (i.e., bicarbonate production is restricted). The results shown in Fig. 5 are consistent with the findings of Lewis et al. (2021) who reported the CDR range of 1.3–8.5 t CO$_2$ ha^{-1} (after 15 years) for six basaltic rocks currently being used in large-scale ERW field trials. This observation again lends confidence that the Stella ERW model accurately estimates the dominant ERW processes.

3.2. Rock processing (life-cycle) variable sensitivity analyses

Conditions for the hypothetical ERW model scenarios discussed below were chosen to accentuate the extent of rock weathering so that the full EWP of the three model rock types would be accounted for (Figs. 6 and 7, and S8). These conditions include the application of fine-grained rock powder (100 μm) to slightly acidic soils (pH 6.5). The predicted CDR ranges for basalt shown in Fig. 6 are higher than those shown in Fig. 5 because we used a rock application rate of 40 t rock ha^{-1}, for the scenarios shown in Fig. 6 and an application rate of 20 t rock ha^{-1} for the runs shown in Fig. 5.

Specifically, Figs. 6, 7 and S8 show results from sensitivity analyses that focus on three life cycle variables: (a-b) the average distance from the rock crushing/milling facility (varied from 5 to 600 km), (c-d) the transportation emissions factors (emissions from rock haulers), which are varied from 0.08 to 0.26 kg CO$_2$ t^{-1} km^{-1}, and (e-f) the electricity emissions factors, which are varied from 0.03 kg CO$_2$ kWh^{-1} (a no fossil

fuels case) up to 0.77 kg CO$_2$ kWh^{-1} (a coal and gas dominated energy mix) (see Tables S6, S7, and S8, Supplementary Information). The rock extraction, loading, and spreading emissions factors (Tables S1 and S2) are included in all model runs shown in Figs. 6, 7 and S8. As with the results shown in Fig. 5, the plotted values are time-integrated. That is, they quantify the overall net CO$_2$ removal at each point in time rather than the instantaneous rate of removal.

Each plot in Figs. 6, 7 and S8 shows the net CO$_2$ balance on the ordinate and the time after rock powder application on the abscissa. Each scenario (model case) is represented by a single curve that accounts for all biogeochemical and life cycle variables. The light gray line is the net zero threshold. So, values above the line represent net positive emissions, and values below the line represent carbon dioxide removal. The dotted line at the bottom of the plots is the rock's EWP (calculated using Equation (6)). Key variable settings for each run are noted in the upper part of each graph. All other variables are set to their default values (Table 5).

Fig. 6a shows results for scenarios where the average transport distance varies from 5 to 600 km. The perhaps unrealistically long transport distance of 600 km is used as a bounding case to show how much this variable could impact the projected CDR. All runs fall below net zero in less than two years, and over ten years, the predicted CDR values range from 12.7 t CO$_2$ ha^{-1} for the 5 km case down to around 8.7 t CO$_2$ ha^{-1} for the 600 km case. Fig. 6b shows the same scenarios as 6a but with the biological index (NPP$_n$) set to 0.1 rather than 1.0. This largely abiotic case shows considerably lower CDR. For example, the 5 km case goes from a drawdown of around 12.7 t CO$_2$ ha^{-1} for the biotic case (NPP$_n$ = 1.0) to a drawdown of approximately 4.2 t CO$_2$ ha^{-1} for the abiotic case (NPP$_n$ = 0.1). The 600 km, low NPP$_n$ scenario results in net positive emissions for the first nine years after amendment and results in a 10-year CDR of less than 1.0 t CO$_2$ ha^{-1}.

Fig. 6c and d shows scenarios in which the rock hauler emissions factors are varied (see Table S3, Supplementary Information). The 10-year net CDR predicted for a scenario using low-efficiency (high emissions) rock haulers is around 7.5 t CO$_2$ ha^{-1} and remains net positive for the project's first two years (Fig. 6c). Using more efficient trucks (i.e., 0.08 kg CO$_2$ t^{-1} km^{-1}) results in a long-term CDR of approximately 11.1 t CO$_2$ ha^{-1}, and the project begins consuming CO$_2$ (reaches net zero) around six months after applying the rock powder (Fig. 6c). Fig. 6d shows the same scenarios using a lower biological function index of (NPP$_n$) of 0.1. Again, this largely abiotic case significantly decreases predicted CDR, with the low hauler efficiency scenario remaining net positive for the entire 10-year monitoring interval. Using the more efficient rock-hauling trucks results in the project reaching net neutrality around three years after application and achieving a 10-year CDR of 2.7 t CO$_2$ ha^{-1}. The results of this run demonstrate the importance of optimizing biogeochemical and life cycle variables. In this case, using energy-inefficient rock haulers and a long transport distance from the mine to the field resulted in net positive emissions for the hypothetical ERW project.

To account for how the electricity required for rock milling impacts CDR predictions, the model was run for a P80 grain size of 10 μm (Fig. 6e) and 1 μm (Fig. 6f). For the 10 μm case, the use of the high electricity emissions factor (0.77 kg CO$_2$ kWh^{-1}) leads to a 10-year CDR of 9.8 t CO$_2$ ha^{-1}, while the no-fossil-fuel case (0.03 kg CO$_2$ kWh^{-1}) results in a 10-year CDR of 11.8 t CO$_2$ ha^{-1}. This difference becomes considerably greater for the 1 μm scenario. For the high fossil fuel emissions factor (0.77 kg CO$_2$ kWh^{-1}), the predicted 10-year CDR is 6.5 t CO$_2$ ha^{-1}, while the no-fossil-fuel scenario yields a 10-year CDR of 12.4 t CO$_2$ ha^{-1}. The life-cycle variable sensitivity analyses for the dunite model rock are shown in Fig. S8, Supplementary Information. The dunite results have the same overall trends as the basalt runs shown in Fig. 6 and discussed above. The main difference is that the dunite EMP and dissolution rates are greater, so it reaches maximum CDR values more rapidly than basalt.

Fig. 7 shows the life-cycle sensitivity analyses for the basaltic

andesite. The results for this model rock show lower overall CDR projections because of its relatively low weathering rate and low EWP (see Table 3 and Fig. 3). Fig. 7a indicates that even using a low transport distance of 5 km, the predicted CDR for basaltic andesite is only 2.6 t CO_2 ha^{-1} after ten years. And for the average transport distance of 600 km, the projected CDR remains below 1 t CO_2 ha^{-1} for ten years, and the project would take over five years to reach net neutral emissions. Running these same scenarios with an $NPP_n = 0.1$ (the "abiotic" case, 7b) results in significant net positive emissions for the 300 km and 600 km rock transport scenarios, and the 5 km scenario achieves a long-term CDR of only 0.6 t CO_2 ha^{-1}.

For cases with variable transport emissions factors (i.e., different rock hauler efficiencies, 7c and 7d), it is observed that if efficient trucks are used (0.08 kg CO_2 t^{-1} km^{-1}), the operation may achieve a CDR of around 1.8 t CO_2 ha^{-1} at ten years (assuming an average transport distance of 500 km). Using low-efficiency (high emissions) haulers results in net positive emissions for over nine years following rock application (Fig. 7c). Running the same scenarios for a low NPP_n value (7d) results in an unviable ERW operation. In this case, the slow abiotic rock weathering results in positive CO_2 emissions for all scenarios.

Decreasing the P80 grain size down to 10 μm helps increase the projected CDR for basaltic andesite to around 2.7 t CO_2 ha^{-1} for the clean energy case (0.03 kg CO_2 kWh^{-1}) and to about 1.7 t CO_2 ha^{-1} for the high emissions case (Fig. 7e). These scenarios would require around 0.5 years and 1.5 years to achieve net neutrality (respectively). Milling the rock down to a P80 grain size of 1 μm results in a projected CDR of approximately 2.7 t CO_2 ha^{-1} for the renewable energy case (0.03 kg CO_2 kWh^{-1}), and approximately 1.2 t CO_2 ha^{-1} for the intermediate energy mix (0.41 kg CO_2 kWh^{-1}) (Fig. 7f). The fossil-fuel-dominated energy case (0.77 kg CO_2 kWh^{-1}) remains net positive and is thus an unviable ERW scenario due to emissions from rock milling equipment.

Comparing the results from the basalt and basaltic andesite life-cycle sensitivity runs (Figs. 6 and 7) underscores the impact that dissolution behavior (i.e., mineralogy) and enhanced weathering potential (i.e., bulk composition) have on predicted CDR values and, thus on the potential viability of a given ERW project. These sensitivity runs also highlight the significant role biological factors could play in the possible failure or success of a particular ERW campaign.

Although the plant and rhizosphere biological processes are not explicitly modeled in the Stella ERW code, it is clear from sensitivity runs discussed above (Figs. 6, 7 and S8) that biology plays a critical role in the effectiveness of ERW as a CDR strategy. The results support the notion that ERW is ultimately a biological intervention. Therefore, field research focusing on the dynamic interplay between biological and geochemical processes will be essential for maximizing the global potential of EWR as a global CDR methodology.

3.3. Implications for a large-scale ERW application

To demonstrate how the observations discussed above impact predicted CDR values at larger scales, we applied the results from the basalt model runs (Fig. 6a) to a hypothetical large-scale ERW project in Brazil. This large-scale operation assumes that basalt rock powder is applied to 25% and 75% of Brazilian agricultural land, which is approximately 1.65×10^7 and 4.95×10^7 ha, respectively (FAOSTAT, 2023). This large-scale model assumes an application rate of 40 t ha^{-1}, rock powder with a P80 grain size of 100 μm. The initial soil pH is 6.5. This model run also assumes a 300 km distance between the mine and the field. The model predicts that this large-scale project would achieve net neutral emissions within half a year of rock application. The initial positive emissions from mining, rock processing, and transportation to the field are approximately 0.04 Gt CO_2 for the 25% case and 0.12 Gt CO_2 for the 75% case. As shown in Fig. 8, after ten years, the cumulative CDR for the 25% Brazilian cropland case is approximately 0.18 Gt CO_2 and approximately 0.53 Gt CO_2 for the 75% cropland coverage scenario.

The net ERW CDR for Brazil has been previously estimated as approximately 0.1 Gt CO_2 yr^{-1} for 25% cropland coverage and approximately 0.2 Gt CO_2 yr^{-1} for 75% cropland coverage (Beerling et al., 2020). The yearly CDR potentials calculated by the Stella ERW model vary with time due to the nonlinear nature of the system; however, they are (in a general sense) consistent with the estimates of Beerling et al. (2020). For example, within the first two years, the net CDR rate predicted by the Stella ERW model for the Brazil scenario is 0.1 Gt CO_2 yr^{-1}, assuming rock powder is applied to 75% of the cropland. This result falls below the range given by Beerling et al. (2020); however, given the differences in geochemical assumptions and modeling approach, the results are not significantly discrepant. This again shows that the Stella ERW model produces results similar to previous work and thus represents a potentially useful reduced-order modeling tool for scoping studies and variable co-optimization for potential ERW projects.

4. Conclusions

The carbon dioxide removal (CDR) potential of enhanced rock weathering (ERW) depends on dynamic interactions between key biogeochemical and life-cycle variables. A reduced order systems model was developed to investigate the impacts of several key variables for a series of hypothetical ERW applications. This paper discussed the development of the model, compared results to ERW field tests, and presented findings from a set of variable sensitivity analyses.

The model accounts for the following variables.

- Rock composition, mineralogy, grain size distribution, rock powder surface area, application rate (t ha^{-1}), and enhanced weathering potential (i.e., kg CO_2 consumed per tonne of rock),
- Soil pH, temperature, and the saturation index of pore solutions,
- Rock transport distances (i.e., from the mine to the crushing/milling facility and from the crushing facility to the field site),
- Carbon dioxide emissions from rock extraction (i.e., drilling and use of explosives),
- Transportation emissions factors for different rock haulers,
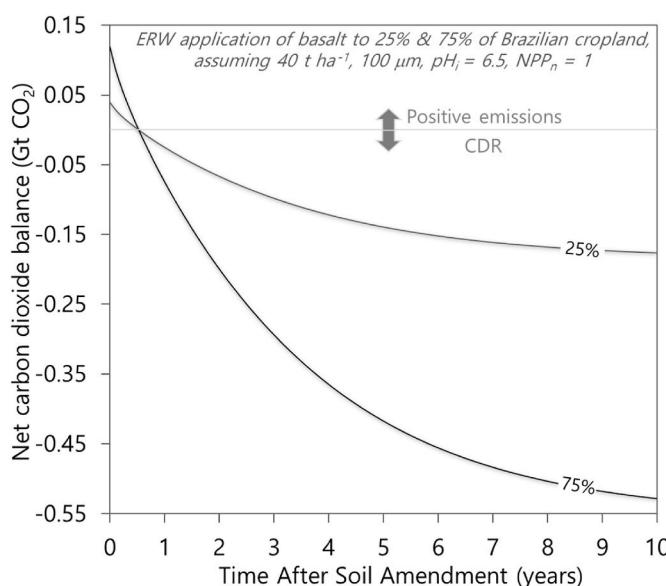- Electrical energy emissions factors that account for CO_2 emissions from rock crushing and milling.

Fig. 8. Model runs from Fig. 6a (basalt, 40 t ha^{-1}, 100 μm, pH$_i$ = 6.5, NPP$_n$ = 1) extrapolated to a large-scale ERW application in Brazil covering 25% and 75% of available cropland. The runs in this plot assume an average distance of 300 km from the mine to the field.

- Carbon dioxide emissions from rock powder application to agricultural fields.

Model results generally agreed with data from ERW laboratory, mesocosm, and field tests (Fig. 4). The model sensitivity analyses predicted CDR values ranging from 1 to 10 t CO_2 ha^{-1} (depending on conditions) for basalt and dunite model rock types over ten years (Fig. 6 and S8). When applied to a large-scale scenario for which 25% and 75% of Brazilian cropland was used for ERW, the model predicts CO_2 drawdowns of 0.18 Gt and 0.53 Gt over ten years.

Model scenarios using a hypothetical basaltic andesite showed a lower projected CDR range of zero to around 2.6 t CO_2 ha^{-1} over a 10-year interval. Scenarios in which basaltic andesite rock powder was combined with low efficiency (i.e., high emission factor) rock haulers and an average rock transport distance of >300 km resulted in net positive emissions for ten years following rock application (Fig. 7). Comparing the results for the basalt and basaltic andesite life-cycle sensitivity runs (Figs. 6 and 7) underscores the impact that dissolution behavior (i.e., mineralogy) and enhanced weathering potential (i.e., bulk composition) have on predicted CDR values and, thus on the viability of a given ERW project.

Any of the variables included in the model can significantly impact the CDR capacity of a given ERW application (Fig. 5); however, it is noted that the biological function, which is a bulk term accounting for macro and microbiological rhizosphere processes, plays a central role (Figs. 6 and 7). When the net primary production index (the main parameter in the biological function) is low, the predicted CDR values are more than a factor of 2 lower than for high NPP cases. This underscores the importance of investigating how site-specific plant and soil biological processes will impact rock weathering for a particular ERW application and suggests that ERW is essentially a biological intervention.

Modeling results show that a combination of inappropriate rock type (e.g., low enhanced weathering potential or slow weathering rates for specific conditions) and suboptimal life cycle issues (e.g., long rock transport distances and high vehicle emissions factors) can result in net positive CO_2 emissions for a 10-year ERW project (Fig. 7). Thus, the primary conclusion of this study is that the co-optimization of geochemical, biological, and life-cycle variables is essential for the successful implementation of ERW applications.

Role of the funding source

This research was performed under the auspices of Remineralize the Earth, a 501(c)(3) non-profit organization based in Northampton, Massachusetts, and founded in 1995 by Joanna Campe.

CRediT authorship contribution statement

James Jerden: Conceptualization, Formal analysis, Investigation, Methodology, Resources, Software, Supervision, Validation, Visualization, Writing – original draft, Writing – review & editing. **Meteb Mejbel:** Conceptualization, Writing – review & editing. **Antonio Nilson Zamunér Filho:** Conceptualization, Resources, Writing – review & editing. **Monica Carroll:** Conceptualization, Methodology, Resources, Writing – review & editing. **Joanna Campe:** Conceptualization, Project administration, Resources, Writing – review & editing.

Declaration of competing interest

The authors declare that they have no known competing financial interests or personal relationships that could have appeared to influence the work reported in this paper.

Appendix A. Supplementary data

Supplementary data to this article can be found online at https://doi.org/10.1016/j.apgeochem.2024.106002.

References

Akter, M., Akagi, T., 2010. Dependence of plant-induced weathering of basalt and andesite on nutrient conditions. Geochem. J. 44, 137–150. https://doi.org/10.2343/geochemj.1.0052.

Akter, M., Akagi, T., 2005. Effect of fine root contact on plant-induced weathering of basalt. Soil Sci. Plant Nutr. 51, 861–871. https://doi.org/10.1111/j.1747-0765.2005.tb00121.x.

Amann, T., Hartmann, J., Struyf, E., de Oliveira Garcia, W., Fischer, E.K., Janssens, I., Meire, P., Schoelynck, J., 2020. Enhanced Weathering and related element fluxes – a cropland mesocosm approach. Biogeosciences 17, 103–119. https://doi.org/10.5194/bg-17-103-2020.

Anda, M., Shamsuddin, J., Fauziah, C.I., 2015. Improving chemical properties of a highly weathered soil using finely ground basalt rocks. Catena 124, 147–161. https://doi.org/10.1016/j.catena.2014.09.012.

Anda, M., Shamsuddin, J., Fauziah, C.I., Omar, S.R.S., 2009. Dissolution of ground basalt and its effect on oxisol chemical properties and cocoa growth. Soil Sci. 174, 264. https://doi.org/10.1097/SS.0b013e3181a56928.

Arrhenius, S., Holden, E.S., 1897. On the influence of carbonic acid in the air upon the temperature of the Earth. Publ. Astron. Soc. Pac. 9, 14–24.

Banfield, J.F., Barker, W.W., Welch, S.A., Taunton, A., 1999. Biological impact on mineral dissolution: application of the lichen model to understanding mineral weathering in the rhizosphere. Proc. Natl. Acad. Sci. USA 96, 3404–3411. https://doi.org/10.1073/pnas.96.7.3404.

Basak, B.B., Sarkar, B., Biswas, D.R., Sarkar, S., Sanderson, P., Naidu, R., 2017. Chapter three - bio-intervention of naturally occurring silicate minerals for alternative source of potassium: challenges and opportunities. In: Sparks, D.L. (Ed.), Advances in Agronomy. Academic Press, pp. 115–145. https://doi.org/10.1016/bs.agron.2016.10.016.

Beerling, D.J., Epihov, D.Z., Kantola, I.B., Masters, M.D., Reershemius, T., Planavsky, N.J., Reinhard, C.T., Jordan, J.S., Thorne, S.J., Weber, J., Val Martin, M., Freckleton, R.P., Hartley, S.E., James, R.H., Pearce, C.R., DeLucia, E.H., Banwart, S.A., 2024. Enhanced weathering in the US Corn Belt delivers carbon removal with agronomic benefits. Proc. Natl. Acad. Sci. USA 121 (9), e2319436121. https://doi.org/10.1073/pnas.2319436121.

Beerling, D.J., Kantzas, E.P., Lomas, M.R., Wade, P., Eufrasio, R.M., Renforth, P., Sarkar, B., Andrews, M.G., James, R.H., Pearce, C.R., Mercure, J.-F., Pollitt, H., Holden, P.B., Edwards, N.R., Khanna, M., Koh, L., Quegan, S., Pidgeon, N.F., Janssens, I.A., Hansen, J., Banwart, S.A., 2020. Potential for large-scale CO_2 removal via enhanced rock weathering with croplands. Nature 583, 242–248. https://doi.org/10.1038/s41586-020-2448-9.

Beerling, D.J., Leake, J.R., Long, S.P., Scholes, J.D., Ton, J., Nelson, P.N., Bird, M., Kantzas, E., Taylor, L.L., Sarkar, B., Kelland, M., DeLucia, E., Kantola, I., Müller, C., Rau, G., Hansen, J., 2018. Farming with crops and rocks to address global climate, food and soil security. Nat. Plants 4, 138–147. https://doi.org/10.1038/s41477-018-0108-y.

Berge, H.F.M. ten, Meer, H.G. van der, Steenhuizen, J.W., Goedhart, P.W., Knops, P., Verhagen, J., 2012. Olivine Weathering in Soil, and Its Effects on Growth and Nutrient Uptake in Ryegrass (Lolium perenne L.): A Pot Experiment. PLOS ONE 7, e42098. https://doi.org/10.1371/journal.pone.0042098.

Berner, R.A., Lasaga, A.C., Garrels, R.M., 1983. The carbonate-silicate geochemical cycle and its effect on atmospheric carbon dioxide over the past 100 million years. Am. J. Sci. 283, 641–683. https://doi.org/10.2475/ajs.283.7.641.

Blanc-Betes, E., Kantola, I.B., Gomez-Casanovas, N., Hartman, M.D., Parton, W.J., Lewis, A.L., Beerling, D.J., DeLucia, E.H., 2021. In silico assessment of the potential of basalt amendments to reduce N2O emissions from bioenergy crops. GCB Bioenergy 13, 224–241. https://doi.org/10.1111/gcbb.12757.

Bond, F.C., 1952. The third theory of comminution. Trans. AIME Min. Eng 193, 484–494.

Box, G.E.P., 1979. Robustness in the strategy of scientific model building. In: Launer, R.L., Wilkinson, G.N. (Eds.), Robustness in Statistics. Academic Press, pp. 201–236. https://doi.org/10.1016/B978-0-12-438150-6.50018-2.

Boyle, J.R., Voigt, G.K., 1973. Biological weathering of silicate minerals. Plant Soil 38, 191–201. https://doi.org/10.1007/BF00011226.

Brantley, S.L., 2008. Kinetics of Mineral Dissolution. In: Brantley, S.L., Kubicki, J.D., White, A.F. (Eds.), Kinetics of Water-Rock Interaction. Springer, New York, NY, pp. 151–210. https://doi.org/10.1007/978-0-387-73563-4_5.

Brantley, S.L., Shaughnessy, A., Lebedeva, M.I., Balashov, V.N., 2023. How temperature-dependent silicate weathering acts as Earth's geological thermostat. Science 379, 382–389. https://doi.org/10.1126/science.add2922.

Brazil, 2013. Law n° 12,890/2013 of december 10, 2013 - amends law n° 6,894 of december 16, 1980, distrito federal. https://www.planalto.gov.br/ccivil_03/_ato2011-2014/2013/lei/l12890.htm (in Portuguese).

Bullock, L.A., Alcalde, J., Tornos, F., Fernandez-Turiel, J.-L., 2023. Geochemical carbon dioxide removal potential of Spain. Sci. Total Environ. 867, 161287 https://doi.org/10.1016/j.scitotenv.2022.161287.

Bullock, L.A., James, R.H., Matter, J., Renforth, P., Teagle, D.A.H., 2021. Global carbon dioxide removal potential of waste materials from metal and diamond mining. Front. Clim. 3.

Busato, J.G., Santos, L.F. dos, Monteiro de Paula, A., Fabriz Sodré, F., de Oliveira, A.L., Dobbss, L.B., Souza Martins, É. de Jindo, K., 2022. Can co-application of silicate rock powder and humic-like acids increase nutrient uptake and plant growth in weathered tropical soil? Acta Agric. Scand. Sect. B Soil Plant Sci 72, 761–774. https://doi.org/10.1080/09064710.2022.2078222.

Calabrese, S., Wild, B., Bertagni, M.B., Bourg, I.C., White, C., Aburto, F., Cipolla, G., Noto, L.V., Porporato, A., 2022. Nano- to global-scale uncertainties in terrestrial enhanced weathering. Environ. Sci. Technol. 56, 15261–15272. https://doi.org/10.1021/acs.est.2c03163.

Campe, J., Mejbel, M., Patskowski, D., Filho, A.N.Z., n.d. Remineralization for a Healthy Planet. Remineralize the Earth white paper report, Northhampton MA, July 19 2022, 39–p.

Chen, A., Chen, Z., Qiu, Z., Lin, B.-L., 2023. Experimentally-calibrated estimation of CO_2 removal potentials of enhanced weathering. Sci. Total Environ. 900, 165766 https://doi.org/10.1016/j.scitotenv.2023.165766.

Chesworth, W., Macias-Vazquenz, F., Acquaye, D., Thompson, E., 1983. Agricultural alchemy: stones into bread. Episodes J. Int. Geosci. 6, 3–7. https://doi.org/10.18814/epiiugs/1983/v6i1/002.

Chiaravalloti, I., Theunissen, N., Zhang, S., Wang, J., Sun, F., Ahmed, A.A., Pihlap, E., Reinhard, C.T., Planavsky, N.J., 2023. Mitigation of soil nitrous oxide emissions during maize production with basalt amendments. Front. Clim. 5.

Choi, W.-J., Park, H.-J., Cai, Y., Chang, S.X., 2021. Environmental risks in atmospheric CO_2 removal using enhanced rock weathering are overlooked. Environ. Sci. Technol. 55, 9627–9629. https://doi.org/10.1021/acs.est.1c02505.

Conceição, L.T., Silva, G.N., Holsback, H.M.S., Oliveira, C. de F., Marcante, N.C., Martins, É. de S., Santos, F.L. de S., Santos, E.F., 2022. Potential of basalt dust to improve soil fertility and crop nutrition. J. Agric. Food Res. 10, 100443 https://doi.org/10.1016/j.jafr.2022.100443.

de Aquino, J.M., Taniguchi, C.A.K., Magini, C., Berni, G.V., 2020. The potential of alkaline rocks from the Fortaleza volcanic province (Brazil) as natural fertilizers. J. South Am. Earth Sci. 103, 102800 https://doi.org/10.1016/j.jsames.2020.102800.

Deng, H., Sonnenthal, E., Arora, B., Breunig, H., Brodie, E., Kleber, M., Spycher, N., Nico, P., 2023. The environmental controls on efficiency of enhanced rock weathering in soils. Sci. Rep. 13, 9765. https://doi.org/10.1038/s41598-023-36113-4.

Dietzen, C., Harrison, R., Michelsen-Correa, S., 2018. Effectiveness of enhanced mineral weathering as a carbon sequestration tool and alternative to agricultural lime: an incubation experiment. Int. J. Greenh. Gas Control 74, 251–258. https://doi.org/10.1016/j.ijggc.2018.05.007.

Drever, J.I., Stillings, L.L., 1997. The role of organic acids in mineral weathering. Colloids Surf. Physicochem. Eng. Asp., Aquatic Colloid and Surface Chemistry 120, 167–181. https://doi.org/10.1016/S0927-7757(96)03720-X.

Dupla, X., Möller, B., Baveye, P.C., Grand, S., 2023. Potential accumulation of toxic trace elements in soils during enhanced rock weathering. Eur. J. Soil Sci. 74, e13343 https://doi.org/10.1111/ejss.13343.

Edwards, D.P., Lim, F., James, R.H., Pearce, C.R., Scholes, J., Freckleton, R.P., Beerling, D.J., 2017. Climate change mitigation: potential benefits and pitfalls of enhanced rock weathering in tropical agriculture. Biol. Lett. 13, 20160715 https://doi.org/10.1098/rsbl.2016.0715.

Eufrasio, R.M., Kantzas, E.P., Edwards, N.R., Holden, P.B., Pollitt, H., Mercure, J.-F., Koh, S.C.L., Beerling, D.J., 2022. Environmental and health impacts of atmospheric CO_2 removal by enhanced rock weathering depend on nations' energy mix. Commun. Earth Environ. 3, 1–13. https://doi.org/10.1038/s43247-022-00436-3.

Fabricius, K.E., 2005. Effects of terrestrial runoff on the ecology of corals and coral reefs: review and synthesis. Mar. Pollut. Bull. 50, 125–146. https://doi.org/10.1016/j.marpolbul.2004.11.028.

Fang, Q., Lu, A., Hong, H., Kuzyakov, Y., Algeo, T.J., Zhao, L., Olshansky, Y., Moravec, B., Barrientes, D.M., Chorover, J., 2023. Mineral weathering is linked to microbial priming in the critical zone. Nat. Commun. 14, 345. https://doi.org/10.1038/s41467-022-35671-x.

FAOSTAT [WWW Document], n.d. URL https://www.fao.org/faostat/en/#search/cropland (accessed 8.December.2023)..

Fyfe, W.S., Leonardos, O.H., Theodoro, S.H., 2006. Sustainable farming with native rocks: the transition without revolution. An. Acad. Bras. Ciênc. 78, 715–720. https://doi.org/10.1590/S0001-37652006000400007.

Gastmans, D., Hutcheon, I., Menegário, A.A., Chang, H.K., 2016. Geochemical evolution of groundwater in a basaltic aquifer based on chemical and stable isotopic data: case study from the Northeastern portion of Serra Geral Aquifer, São Paulo state (Brazil). J. Hydrol. 535, 598–611. https://doi.org/10.1016/j.jhydrol.2016.02.016.

Gaucher, Y., Tanaka, K., Johansson, D., Goll, D., Ciais, P., 2023. Leveraging ecosystems responses to enhanced weathering in mitigation scenarios. https://doi.org/10.21203/rs.3.rs-3145606/v1.

Gillman, G.P., 1980. The effect of crushed basalt scoria on the cation Exchange properties of a highly weathered soil. Soil Sci. Soc. Am. J. 44, 465–468. https://doi.org/10.2136/sssaj1980.03615995004400030005x.

Gillman, G.P., Burkett, D.C., Coventry, R.J., 2002. Amending highly weathered soils with finely ground basalt rock. Appl. Geochem. 17, 987–1001. https://doi.org/10.1016/S0883-2927(02)00078-1.

Goldberg, P., Chen, Z.-Y., O'Connor, W., Walters, R., Ziock, H., 2001. CO_2 Mineral Sequestration Studies in the U.S. (No. DOE/NETL-2001/1144). National Energy Technology Laboratory, Pittsburgh, PA (United States).

Goll, D.S., Ciais, P., Amann, T., Buermann, W., Chang, J., Eker, S., Hartmann, J., Janssens, I., Li, W., Obersteiner, M., Penuelas, J., Tanaka, K., Vicca, S., 2021. Potential CO_2 removal from enhanced weathering by ecosystem responses to powdered rock. Nat. Geosci. 14, 545–549. https://doi.org/10.1038/s41561-021-00798-x.

Gudbrandsson, S., Wolff-Boenisch, D., Gislason, S.R., Oelkers, E.H., 2011. An experimental study of crystalline basalt dissolution from $2 \leqslant pH \leqslant 11$ and temperatures from 5 to 75°C. Geochem. Cosmochim. Acta 75, 5496–5509. https://doi.org/10.1016/j.gca.2011.06.035.

Guo, F., Wang, Y., Zhu, H., Zhang, C., Sun, H., Fang, Z., Yang, J., Zhang, L., Mu, Y., Man, Y.B., Wu, F., 2023. Crop productivity and soil inorganic carbon change mediated by enhanced rock weathering in farmland: a comparative field analysis of multi-agroclimatic regions in central China. Agric. Syst. 210, 103691 https://doi.org/10.1016/j.agsy.2023.103691.

Campe, 2014. In: Goreau, T.J., Larson, R.W., Campe, J. (Eds.), Potential of Remineralization as a Global Movement in "Geotherapy: Innovative Methods of Soil Fertility Restoration, Carbon Sequestration, and Reversing CO2 Increase. CRC Press, Boca Raton, pp. 81–110. https://doi.org/10.1201/b13788.

Haque, F., Santos, R.M., Chiang, Y.W., 2021. Urban farming with enhanced rock weathering as a prospective climate stabilization wedge. Environ. Sci. Technol. 55, 13575–13578. https://doi.org/10.1021/acs.est.1c04111.

Haque, F., Chiang, Y.W., Santos, R.M., 2020. Risk assessment of Ni, Cr, and Si release from alkaline minerals during enhanced weathering. Open Agri. 5 (1), 166–175. https://doi.org/10.1515/opag-2020-0016.

Harley, A.D., Gilkes, R., 2000. Factors influencing the release of plant nutrient elements from silicate rock powders: a geochemical overview. Nutrient Cycl. Agroecosyst. 56, 11–36. https://doi.org/10.1023/A:1009859309453.

Hartmann, J., West, A.J., Renforth, P., Köhler, P., De La Rocha, C.L., Wolf-Gladrow, D.A., Dürr, H.H., Scheffran, J., 2013a. Enhanced chemical weathering as a geoengineering strategy to reduce atmospheric carbon dioxide, supply nutrients, and mitigate ocean acidification. Rev. Geophys. 51, 113–149. https://doi.org/10.1002/rog.20004.

Hartmann, J., West, A.J., Renforth, P., Köhler, P., De La Rocha, C.L., Wolf-Gladrow, D.A., Dürr, H.H., Scheffran, J., 2013b. Enhanced chemical weathering as a geoengineering strategy to reduce atmospheric carbon dioxide, supply nutrients, and mitigate ocean acidification. Rev. Geophys. 51, 113–149. https://doi.org/10.1002/rog.20004.

Henderson, M.E.K., Duff, R.B., 1963. The release of metallic and silicate ions from minerals, rocks, and soils by fungal activity. J. Soil Sci. 14, 236–246. https://doi.org/10.1111/j.1365-2389.1963.tb00949.x.

Hensel, J., 1894. Bread from Stones: A New and Rational System of Land Fertilization and Physical Regeneration (Translated from the German, 1894). A.J. Tafel, T.B. and H.B. Cochran, Printers, Lancaster, PA.

Heřmanská, M., Voigt, M.J., Marieni, C., Declercq, J., Oelkers, E.H., 2022. A comprehensive and internally consistent mineral dissolution rate database: Part I: primary silicate minerals and glasses. Chem. Geol. 597, 120807 https://doi.org/10.1016/j.chemgeo.2022.120807.

Hoffland, E., Kuyper, T., Wallander, H., Plassard, C., Gorbushina, A., Haselwandter, K., Holmstrom, S., Landeweert, R., Lundstrom, U.S., Rosling, A., Sen, R., Smits, M., Hees, Breemen, 2004. The role of fungi in weathering. Front. Ecol. Environ. https://doi.org/10.1890/1540-9295(2004)002[0258:TROFIW]2.0.CO;2.

Huang, P.M., Schnitzer, M., 1986. Interactions of Soil Minerals with Natural Organics and Microbes. SSSA special publication. The Soil Science Society of America, Madison, Wis., USA.

IPCC, 2018. Global Warming of 1.5°C: IPCC Special Report on Impacts of Global Warming of 1.5°C above Pre-Industrial Levels in Context of Strengthening Response to Climate Change, Sustainable Development, and Efforts to Eradicate Poverty. Cambridge University Press, Cambridge. https://doi.org/10.1017/9781009157940.

IPCC, 2022a. Climate change 2022: impacts, adaptation and vulnerability. Contrib. Work. Group Sixth Assess. Rep. Intergovern. Panel Clim. Change. https://doi.org/10.1017/9781009157926.

Kantola, I.B., Masters, M.D., Beerling, D.J., Long, S.P., DeLucia, E.H., 2017. Potential of global croplands and bioenergy crops for climate change mitigation through deployment for enhanced weathering. Biol. Lett. 13, 20160714 https://doi.org/10.1098/rsbl.2016.0714.

Kantzas, E.P., Val Martin, M., Lomas, M.R., Eufrasio, R.M., Renforth, P., Lewis, A.L., Taylor, L.L., Mecure, J.-F., Pollitt, H., Vercoulen, P.V., Vakilifard, N., Holden, P.B., Edwards, N.R., Koh, L., Pidgeon, N.F., Banwart, S.A., Beerling, D.J., 2022. Substantial carbon drawdown potential from enhanced rock weathering in the United Kingdom. Nat. Geosci. 15, 382–389. https://doi.org/10.1038/s41561-022-00925-2.

Kanzaki, Y., Planavsky, N.J., Reinhard, C.T., 2023. New estimates of the storage permanence and ocean co-benefits of enhanced rock weathering. PNAS Nexus 2, pgad059. https://doi.org/10.1093/pnasnexus/pgad059.

Kelland, M.E., Wade, P.W., Lewis, A.L., Taylor, L.L., Sarkar, B., Andrews, M.G., Lomas, M.R., Cotton, T.E.A., Kemp, S.J., James, R.H., Pearce, C.R., Hartley, S.E.,

Hodson, M.E., Leake, J.R., Banwart, S.A., Beerling, D.J., 2020. Increased yield and CO₂ sequestration potential with the C4 cereal Sorghum bicolor cultivated in basaltic rock dust-amended agricultural soil. Global Change Biol. 26, 3658–3676. https://doi.org/10.1111/gcb.15089.

Kemp, P., Sear, D., Collins, A., Naden, P., Jones, I., 2011. The impacts of fine sediment on riverine fish. Hydrol. Process. 25, 1800–1821. https://doi.org/10.1002/hyp.7940.

Kemp, S.J., Lewis, A.L., Rushton, J.C., 2022. Detection and quantification of low levels of carbonate mineral species using thermogravimetric-mass spectrometry to validate CO₂ drawdown via enhanced rock weathering. Appl. Geochem. 146, 105465 https://doi.org/10.1016/j.apgeochem.2022.105465.

Klemme, A., Rixen, T., Müller, M., Notholt, J., Warneke, T., 2022. Destabilization of carbon in tropical peatlands by enhanced weathering. Commun. Earth Environ. 3, 1–9. https://doi.org/10.1038/s43247-022-00544-0.

Knapp, W.J., Stevenson, E.I., Renforth, P., Ascough, P.L., Knight, A.C.G., Bridgestock, L., Bickle, M.J., Lin, Y., Riley, A.L., Mayes, W.M., Tipper, E.T., 2023. Quantifying CO₂ removal at enhanced weathering sites: a multiproxy approach. Environ. Sci. Technol. 57, 9854–9864. https://doi.org/10.1021/acs.est.3c03757.

Köhler, P., Hartmann, J., Wolf-Gladrow, D.A., 2010. Geoengineering potential of artificially enhanced silicate weathering of olivine. Proc. Natl. Acad. Sci. USA 107, 20228–20233. https://doi.org/10.1073/pnas.1000545107.

Koukouzas, N., Koutsovitis, P., Tyrologou, P., Karkalis, C., Arvanitis, A., 2019. Potential for mineral carbonation of CO₂ in pleistocene basaltic rocks in volos region (Central Greece). Minerals 9, 627. https://doi.org/10.3390/min9100627.

Krahl, L.L., Valadares, L.F., Sousa-Silva, J.C., Marchi, G., Martins, É. de S., 2022. Dissolution of silicate minerals and nutrient availability for corn grown successively. Pesqui. Agropecuária Bras. 57, e01467 https://doi.org/10.1590/S1678-3921.pab2022.v57.01467.

Larkin, C.S., Andrews, M.G., Pearce, C.R., Yeong, K.L., Beerling, D.J., Bellamy, J., Benedick, S., Freckleton, R.P., Goring-Harford, H., Sadekar, S., James, R.H., 2022. Quantification of CO₂ removal in a large-scale enhanced weathering field trial on an oil palm plantation in Sabah, Malaysia. Front. Clim. 4.

Lefebvre, D., Goglio, P., Williams, A., Manning, D.A.C., de Azevedo, A.C., Bergmann, M., Meersmans, J., Smith, P., 2019. Assessing the potential of soil carbonation and enhanced weathering through Life Cycle Assessment: a case study for Sao Paulo State, Brazil. J. Clean. Prod. 233, 468–481. https://doi.org/10.1016/j.jclepro.2019.06.099.

Lehmann, J., Possinger, A., 2020. Removal of atmospheric CO₂ by rock weathering holds promise for mitigating climate change. Nature 583, 204–205. https://doi.org/10.1038/d41586-020-01965-7.

Leonardos, O.H., Theodoro, S.H., Assad, M.L., 2000. Remineralization for sustainable agriculture: a tropical perspective from a Brazilian viewpoint. Nutrient Cycl. Agroecosyst. 56, 3–9. https://doi.org/10.1023/A:1009855409700.

Lewis, A.L., Sarkar, B., Wade, P., Kemp, S.J., Hodson, M.E., Taylor, L.L., Yeong, K.L., Davies, K., Nelson, P.N., Bird, M.I., Kantola, I.B., Masters, M.D., DeLucia, E., Leake, J.R., Banwart, S.A., Beerling, D.J., 2021. Effects of mineralogy, chemistry and physical properties of basalts on carbon capture potential and plant-nutrient element release via enhanced weathering. Appl. Geochem. 132, 105023 https://doi.org/10.1016/j.apgeochem.2021.105023.

Maher, K., Steefel, C.I., White, A.F., Stonestrom, D.A., 2009. The role of reaction affinity and secondary minerals in regulating chemical weathering rates at the Santa Cruz Soil Chronosequence, California. Geochem. Cosmochim. Acta 73, 2804–2831. https://doi.org/10.1016/j.gca.2009.01.030.

Manning, D.A.C., Renforth, P., 2013. Passive sequestration of atmospheric CO₂ through coupled plant-mineral reactions in urban soils. Environ. Sci. Technol. 47, 135–141. https://doi.org/10.1021/es301250j.

Manning, D.A.C., Theodoro, S.H., 2020. Enabling food security through use of local rocks and minerals. Extr. Ind. Soc. 7, 480–487. https://doi.org/10.1016/j.exis.2018.11.002.

Marchi, G., Guelfi-Silva, D.R., Malaquias, J.V., Guilherme, L.R.G., Spehar, C.R., Martins, E. de S., 2020. Solubility and availability of micronutrients extracted from silicate agrominerals. Pesqui. Agropecuária Bras. 55, e00807 https://doi.org/10.1590/S1678-3921.pab2020.v55.00807.

Meysman, F.J.R., Montserrat, F., 2017. Negative CO₂ emissions via enhanced silicate weathering in coastal environments. Biol. Lett. 13, 20160905 https://doi.org/10.1098/rsbl.2016.0905.

Moosdorf, N., Renforth, P., Hartmann, J., 2014. Carbon dioxide efficiency of terrestrial enhanced weathering. Environ. Sci. Technol. 48, 4809–4816. https://doi.org/10.1021/es4052022.

Paessler, D., Steffens, R., Hammes, J., Smet, I., 2023. Monitoring CO₂ Concentrations in Soil Gas: A Novel MRV Approach for Cropland-Based ERW?.

Palandri, J., Kharaka, Y., 2004. A Compilation of Rate Parameters of Water-Mineral Interaction Kinetics for Application to Geochemical Modeling, vol. 1068, p. 71.

Pollyea, R.M., Rimstidt, J.D., 2017. Rate equations for modeling carbon dioxide sequestration in basalt. Appl. Geochem. 81, 53–62. https://doi.org/10.1016/j.apgeochem.2017.03.020.

Quirk, J., Andrews, M.Y., Leake, J.R., Banwart, S.A., Beerling, D.J., 2014. Ectomycorrhizal fungi and past high CO₂ atmospheres enhance mineral weathering through increased below-ground carbon-energy fluxes. Biol. Lett. 10, 20140375 https://doi.org/10.1098/rsbl.2014.0375.

Quirk, J., Beerling, D.J., Banwart, S.A., Kakonyi, G., Romero-Gonzalez, M.E., Leake, J.R., 2012. Evolution of trees and mycorrhizal fungi intensifies silicate mineral weathering. Biol. Lett. 8, 1006–1011. https://doi.org/10.1098/rsbl.2012.0503.

Ramos, C.G., Hower, J.C., Blanco, E., Oliveira, M.L.S., Theodoro, S.H., 2022. Possibilities of using silicate rock powder: an overview. Geosci. Front. 13, 101185 https://doi.org/10.1016/j.gsf.2021.101185.

Reershemius, T., Kelland, M.E., Jordan, J.S., Davis, I.R., D'Ascanio, R., Kalderon-Asael, B., Asael, D., Epihov, D.Z., Beerling, D.J., Reinhard, C.T., Planavsky, N.J., 2023. A new soil-based approach for empirical monitoring of enhanced rock weathering rates. https://doi.org/10.48550/arXiv.2302.05004.

Renforth, P., 2019. The negative emission potential of alkaline materials. Nat. Commun. 10, 1401. https://doi.org/10.1038/s41467-019-09475-5.

Renforth, P., 2012. The potential of enhanced weathering in the UK. Int. J. Greenh. Gas Control 10, 229–243. https://doi.org/10.1016/j.ijggc.2012.06.011.

Reynaert, S., Vienne, A., De Boeck, H.J., D'Hose, T., Janssens, I., Nijs, I., Portillo-Estrada, M., Verbruggen, E., Vicca, S., Poblador, S., 2023. Basalt addition improves the performance of young grassland monocultures under more persistent weather featuring longer dry and wet spells. Agric. For. Meteorol. 340, 109610 https://doi.org/10.1016/j.agrformet.2023.109610.

Rinder, T., von Hagke, C., 2021. The influence of particle size on the potential of enhanced basalt weathering for carbon dioxide removal - insights from a regional assessment. J. Clean. Prod. 315, 128178 https://doi.org/10.1016/j.jclepro.2021.128178.

Schatz, A., Cheronis, N.D., Schatz, V., Trelawny, G.S., 1954. Chelation (sequestration) as a biological weathering factor in pedogenesis. Proc. Pa. Acad. Sci. 28, 44–51.

Schuiling, R.D., Krijgsman, P., 2006. Enhanced weathering: an effective and cheap tool to sequester CO₂. Clim. Change 74, 349–354. https://doi.org/10.1007/s10584-005-3485-y.

Seifritz, W., 1990. CO₂ disposal by means of silicates. Nature 345. https://doi.org/10.1038/345486b0, 486–486.

Shamsuddin, J., Panhwar, Q.A., Roslan, I., Fauziah, C.I., Naher, U.A., Hakeem, K.R., 2015. Sustaining cocoa production on oxisols in Malaysia. In: Hakeem, K.R. (Ed.), Crop Production and Global Environmental Issues. Springer International Publishing, Cham, pp. 169–180. https://doi.org/10.1007/978-3-319-23162-4_7.

Sikora, L.J., 2004. Effects of basaltic mineral fines on composting. Waste Manag. 24, 139–142. https://doi.org/10.1016/j.wasman.2003.08.005.

Smith, P., Adams, J., Beerling, D.J., Beringer, T., Calvin, K.V., Fuss, S., Griscom, B., Hagemann, N., Kammann, C., Kraxner, F., Minx, J.C., Popp, A., Renforth, P., Vicente Vicente, J.L., Keesstra, S., 2019. Land-management options for greenhouse gas removal and their impacts on ecosystem services and the sustainable development goals. Annu. Rev. Environ. Resour. 44, 255–286. https://doi.org/10.1146/annurev-environ-101718-033129.

Steinour, H.H., 1959. Some effects of carbon dioxide on mortars and concrete-discussion. J. Am. Concr. Inst. 30, 905–907.

Straaten, P. van, 2022. Distribution of agromineral resources in space and time – a global geological perspective. Pesqui. Agropecuária Bras. 57, e01453 https://doi.org/10.1590/S1678-3921.pab2022.v57.01453.

Strefler, J., Amann, T., Bauer, N., Kriegler, E., Hartmann, J., 2018. Potential and costs of carbon dioxide removal by enhanced weathering of rocks. Environ. Res. Lett. 13, 034010 https://doi.org/10.1088/1748-9326/aaa9c4.

Stubbs, A.R., Paulo, C., Power, I.M., Wang, B., Zeyen, N., Wilson, S., 2022. Direct measurement of CO₂ drawdown in mine wastes and rock powders: implications for enhanced rock weathering. Int. J. Greenh. Gas Control 113, 103554. https://doi.org/10.1016/j.ijggc.2021.103554.

Suhrhoff, T.J., 2022. Phytoprevention of Heavy Metal Contamination from Terrestrial Enhanced Weathering: Can Plants Save the Day? Front. Clim., vol. 3.

Swoboda, P., Döring, T.F., Hamer, M., 2022. Remineralizing soils? The agricultural usage of silicate rock powders: a review. Sci. Total Environ. 807, 150976 https://doi.org/10.1016/j.scitotenv.2021.150976.

Taylor, L.L., Beerling, D.J., Quegan, S., Banwart, S.A., 2017. Simulating carbon capture by enhanced weathering with croplands: an overview of key processes highlighting areas of future model development. Biol. Lett. 13, 20160868 https://doi.org/10.1098/rsbl.2016.0868.

Taylor, L.L., Quirk, J., Thorley, R.M.S., Kharecha, P.A., Hansen, J., Ridgwell, A., Lomas, M.R., Banwart, S.A., Beerling, D.J., 2016. Enhanced weathering strategies for stabilizing climate and averting ocean acidification. Nat. Clim. Change 6, 402–406. https://doi.org/10.1038/nclimate2882.

te Pas, E.E.E.M., Hagens, M., Comans, R.N.J., 2023. Assessment of the enhanced weathering potential of different silicate minerals to improve soil quality and sequester CO₂. Front. Clim. 4, 954064 https://doi.org/10.3389/fclim.2022.954064.

Theodoro, S.H., de Paula Medeiros, F., Ianniruberto, M., Baiocchi Jacobson, T.K., 2021. Soil remineralization and recovery of degraded areas: an experience in the tropical region. J. South Am. Earth Sci. 107, 103014 https://doi.org/10.1016/j.jsames.2020.103014.

Theodoro, S.H., Leonardos, O.H., 2006. The use of rocks to improve family agriculture in Brazil. An. Acad. Bras. Ciênc. 78, 721–730. https://doi.org/10.1590/S0001-37652006000400008.

Urey, H.C., 1952. The planets, their origin and development. Mrs. Hepsa Ely Silliman Memorial Lectures. Yale University Press, New Haven, Conn.

Vakilifard, N., Kantzas, E.P., Edwards, N.R., Holden, P.B., Beerling, D.J., 2021. The role of enhanced rock weathering deployment with agriculture in limiting future warming and protecting coral reefs. Environ. Res. Lett. 16, 094005 https://doi.org/10.1088/1748-9326/ac1818.

Van Straaten, P., 2006. Farming with rocks and minerals: challenges and opportunities. An. Acad. Bras. Ciênc. 78, 731–747. https://doi.org/10.1590/S0001-37652006000400009.

Vanderkloot, E., Ryan, P., 2023. Quantifying the effect of grain size on weathering of basaltic powders: implications for negative emission technologies via soil carbon sequestration. Appl. Geochem. 155, 105728 https://doi.org/10.1016/j.apgeochem.2023.105728.

Verbruggen, E., Struyf, E., Vicca, S., 2021. Can arbuscular mycorrhizal fungi speed up carbon sequestration by enhanced weathering? Plants People Planet 3, 445–453. https://doi.org/10.1002/ppp3.10179.

Vicca, S., Goll, D.S., Hagens, M., Hartmann, J., Janssens, I.A., Neubeck, A., Peñuelas, J., Poblador, S., Rijnders, J., Sardans, J., Struyf, E., Swoboda, P., van Groenigen, J.W., Vienne, A., Verbruggen, E., 2022. Is the climate change mitigation effect of enhanced silicate weathering governed by biological processes? Global Change Biol. 28, 711–726. https://doi.org/10.1111/gcb.15993.

Vienne, A., Poblador, S., Portillo-Estrada, M., Hartmann, J., Ijiehon, S., Wade, P., Vicca, S., 2022. Enhanced weathering using basalt rock powder: carbon sequestration, Co-benefits and risks in a mesocosm study with Solanum tuberosum. Front. Clim. 4.

Vink, J., Giesen, D., Ahlrichs, E., 2022. Olivine weathering in field trials; Effect of natural environmental conditions on mineral dissolution and the potential toxicity of nickel (rapport Deltares).

Vink, J.P.M., Knops, P., 2023. Size-fractionated weathering of olivine, its CO_2-sequestration rate, and ecotoxicological risk assessment of nickel release. Minerals 13, 235. https://doi.org/10.3390/min13020235.

Walker, J.C.G., Hays, P.B., Kasting, J.F., 1981. A negative feedback mechanism for the long-term stabilization of Earth's surface temperature. J. Geophys. Res. Oceans 86, 9776–9782. https://doi.org/10.1029/JC086iC10p09776.

White, A.F., Bullen, T.D., Schulz, M.S., Blum, A.E., Huntington, T.G., Peters, N.E., 2001. Differential Rates of Feldspar Weathering in Granitic Regoliths. Geochimica et Cosmochimica Acta 65 (6), 847–869. https://doi.org/10.1016/S0016-7037(00)00577-9.

White, A.F., Buss, H.L., 2014. 7.4 - natural weathering rates of silicate minerals. In: Holland, H.D., Turekian, K.K. (Eds.), Treatise on Geochemistry, second ed. Elsevier, Oxford, pp. 115–155. https://doi.org/10.1016/B978-0-08-095975-7.00504-0.

Wild, B., Gerrits, R., Bonneville, S., 2022. The contribution of living organisms to rock weathering in the critical zone. npj Mater. Degrad. 6, 1–16. https://doi.org/10.1038/s41529-022-00312-7.

Zaharescu, D.G., Burghelea, C.I., Dontsova, K., Reinhard, C.T., Chorover, J., Lybrand, R., 2020. Biological weathering in the terrestrial system. In: Biogeochemical Cycles. American Geophysical Union (AGU), pp. 1–32. https://doi.org/10.1002/9781119413332.ch1.

Zeebe, R.E., Wolf-Gladrow, D.A., 2009. Carbon dioxide, dissolved (ocean). In: Gornitz, V. (Ed.), Encyclopedia of Paleoclimatology and Ancient Environments, Encyclopedia of Earth Sciences Series. Springer, Netherlands, Dordrecht, pp. 123–127. https://doi.org/10.1007/978-1-4020-4411-3_30.

Zhang, S., Bai, X., Zhao, C., Tan, Q., Luo, G., Wang, J., Li, Q., Wu, L., Chen, F., Li, C., Deng, Y., Yang, Y., Xi, H., 2021. Global CO_2 consumption by silicate rock chemical weathering: its past and future. Earth's Future 9, e2020EF001938. https://doi.org/10.1029/2020EF001938.

Zhang, S., Planavsky, N.J., Katchinoff, J., Raymond, P.A., Kanzaki, Y., Reershemius, T., Reinhard, C.T., 2022. River chemistry constraints on the carbon capture potential of surficial enhanced rock weathering. Limnol. Oceanogr. 67, S148–S157. https://doi.org/10.1002/lno.12244.